Physics – Uspekhi **46** (7) 689 – 715 (2003)

REVIEWS OF TOPICAL PROBLEMS PACS numbers: 62.20.De, 63.20.Pw, **63.50.+x**

Isotope effects in lattice dynamics

V G Plekhanov

DOI: 10.1070/PU2003v046n07ABEH001383

Contents

Abstract. The large number of available stable isotopes and well developed isotope separation technology have enabled growing crystals of C, LiH, ZnO, CuCl, CuBr, Cu_2O, CdS, α-Sn, Ge, Si, etc.with a controlled isotope composition. Experimental and theoretical studies provide evidence that the isotope effect has an influence on the thermal, elastic, and vibrational properties of crystals. In this paper it is shown that in Ge and C crystals isotope effect causes only weak phonon scattering whereas in LiH the scattering potential changes are so strong that they lead to experimentally observable phonon localization. It is emphasized that a systematic description of isotope effects requires that anharmonicity be taken into account.

1. Introduction

The concept of isotopes was introduced by Soddy in 1910 in his studies of radioactivity (see, for example, Ref. [1]). According to Soddy, isotopes are chemical elements having the same atomic number (electric charge of the nucleus), but different atomic mass (number of neutrons). In 1912, Thomson found by mass separation in magnetic and electric fields that neon consisted of two isotopes: ^{20}Ne and ^{22}Ne. About 300 stable and 1000 radioactive isotopes are known today. Some elements are isotopically pure (for example, Co), while others may contain numerous isotopic modifications (for example, Sn has 10 stable isotopes with atomic masses ranging from 112 to 124, while Xe has 23 isotopes, 9 of which are stable) [2].

V G Plekhanov Institute for Computer Engineering and Science
ul. Erika 7a, 10416 Tallinn, Estonia
Tel. (10-372) 648 77 73
E-mail: vgplekhanov@hotmail.com

Received 15 December 2002, revised 19 March 2003
Uspekhi Fizicheskikh Nauk **173** (7) 711 – 738 (2003)
Translated by A V Leonidov; edited by S N Gorin

Isotopes have long been used for different scientific applications, especially in atomic [3] and molecular [4] spectroscopy. It is interesting to note that the isotope shift of the vibration band in oxygen (O – O) was a direct proof of existence of zero-point vibrations [5]. The discovery of zero-point oscillations called for the introduction of the half-integer quantum number in quantum mechanics. It is well known that the energy of zero-point vibrations is different for the ground and the excited electron states, and cannot be changed by any external force. It is the different value of the energy of zero-point vibrations in different isotopes that causes the energy shift of the purely electron transition in molecules with different isotope composition. Moreover, taking into account the interaction between electrons and vibrations (which depends on isotope composition) leads to additional renormalization of electronic terms [5]. Simultaneously, it has been noticed that, already in the description of the isotope shift in the purely electronic transition in molecules (for example, for substitution of deuterium for hydrogen), harmonic approximation of the theory is insufficient [5, 4]. Note that isotope spectroscopy has already resolved quite a few contradictions in nuclear physics [6].

Even more pronounced are isotope effects in solids. A vivid example is provided by experimental data demonstrating that after D substitution for H the change in the transition energy in a solid (for example, LiH) is two orders of magnitude larger than in atomic hydrogen [7]. The first experimental investigations of isotope effects in solids were carried out already in the 1930s. In 1935 Ubbelohde [8] noticed that substitution of one isotope by another leads to changes in vibrational and rotational frequencies of molecules, but does not influence the structure of interatomic potential. In the above-mentioned papers the main emphasis was on studying the isotope effects in structural properties (see also Ref. [9]).

As already mentioned, the existence of many stable and long-lived isotopes allows us to talk about the emergent

spectroscopy of solids with a given and controllable isotope composition. The latter allows us to carry out studies of crystals with varying isotope compositions that previously were simply impossible because of the absence of the object of study. The well-perfected modern technology of isotope separation (see, for example, Ref. [10]) has made it possible to obtain high-purity materials with practically 100% homogeneity in their isotope composition. Besides LiH [11, 12], Cu_2O [13 – 15], ZnO [16, 17], and CdS [18] crystals with varying isotope composition in anionic and cationic sublattices, which were already grown a long time ago, recently crystals of diamond [19, 20], germanium [21, 22], silicon [23, 26], copper chloride and bromide [24, 25], ZnSe, and GaAs [27] have been grown.

Besides traditional applied problems, let us mention new isotope engineering issues such as new media for information recording, fiber optics, doping semiconductors by neutron transmutation, thermosensors from ultrapure materials, quantum computers, and many others of a potentially applied nature (see, for example, [28 – 32]).

Beginning with the classical theory of the isotope defect by Lifshitz [33], the interest in the dynamics of lattices with defects has not weakened in the already more than five decades (see, e.g., the reviews [34 – 40]) that have passed. Such focused attention on the simplest defect problem can be explained, in particular, by the successful application of the methods used in its solution not only to mixed crystals, but also to disordered systems in general [34, 36, 39]. By definition, in the isotope-defect model it is only the mass that changes, the force constant remaining the same [33, 34]. Using numerical methods, Dean [35] and Bell [36] have shown that a spectrum of the disordered system has two characteristic domains: one continuous, related to extended states, and the second spiky, related to the localized ones. The nature of the latter is often related to a single center, pair, and so on, with a subsequent clusterization of defects (see also Refs [41 – 43]). With increasing concentration of isotopes, when interaction between defects becomes essential, in the limit an isotopically mixed crystal is obtained. A mixed systems of this type could maximally correspond to the virtual-crystal model because, at first sight, no changes in the effective charge and force constant should happen in them. As to the dependence of the lattice parameter of the isotopically mixed crystals on isotope concentration, it is, as a rule [23, 44, 45], linear (see, however, Ref. [46]).

Therefore, the simplest isotopically mixed crystals could provide a model bridge between the physical properties of isolated impurity (isotope defect) and the properties of amorphous [47] or fully disordered materials (see also Refs [39, 41]). As the concentration of isotopes can vary in a broad interval ($0 < x < 100\%$), one can hope that this gives a rare chance of tracing the percolation threshold that separates localized states in the phonon spectrum from the extended ones [48, 49]. Not only does the isotope substitution modify the lattice dynamics, but it also allows us to separate the effects due to the isotopic disorder in the crystal lattice from anharmonic processes. Investigations of this kind help in better understanding the phonon decay mechanisms and their influence on other properties of crystals (phonon – phonon interaction, lattice parameter, thermal conductivity, etc.). It is now becoming clear that harmonic approximation is insufficient even at low temperatures. Because of zero vibrations, the influence of anharmonicity does not disappear even at $T = 0$ K. This influence turns out to be most pronounced for small masses of ions (atoms) when zero vibrations are, correspondingly, large (for example, in diamond or lithium hydride). As a result, equilibrium positions do not coincide with the minimum of the potential energy. The role of anharmonicity in various cases and different effects in solids are discussed in extensive reviews [50, 51] and monographs [52, 53]. Here it is appropriate to note that the equilibrium volume of the crystal depends on its isotope composition precisely due to the anharmonic effects and zero vibrations. As was already mentioned, the energy of the latter can be significant and depends only on the nuclear mass.

In the present review we discuss the effects related to the influence of isotope substitution on elastic, thermal and vibrational properties of dielectric and semiconducting crystals. The most pronounced isotope effects are observed, in a wide concentration range, in mixed LiH_xD_{1-x} and $^{12}C_x\,^{13}C_{1-x}$ crystals. This is not puzzling because, first, the H^- and Li^+ ions have the maximal possible ratio of the masses of isotopes. Second, the smallness of ion masses results in relatively large vibration frequencies (this is also true for diamond). Because of this, the observation of quantum properties in many phenomena is, in contrast to other crystals discussed in this review, possible up to room temperature. Third, the deviation from the purely ionic bond in LiH (ionicity equals 0.8 – 1 [54]) results in a significant contribution of noncentral and three-body forces which manifest themselves in the anomalies of elastic and other characteristics.

A brief review of experimental and theoretical results on the lattice dynamics of the LiH_xD_{1-x} crystals in a wide range of concentrations has been made in [55]. Comparing the ionic radii $r_{Li^+} = 0.68$ Å and $r_{H^-} = 1.5$ Å and the lattice parameter $a = 2.042$ Å, one sees that in the lithium hydride the lithium and hydrogen ions significantly overlap. More detailed information on the physicochemical characteristics of lithium hydride can be found in Ref. [56], and that for diamond in Ref. [57]. The common features of the results obtained for C, LiH, ZnO, ZnSe, Cds, CuCl, CuBr, Cu_2O, GaAs, Ge and Si crystals with isotope substitution witnesses the emergence of a new direction in lattice dynamics. Thus, it seems timely to give a brief review of experimental results on the isotope effects in lattice dynamics. A step-by-step comparison with existing theoretical models (see, e.g., Ref. [58]) could not only reveal the degree of agreement (or disagreement), but provide a new impulse both for the development of new theoretical ideas and for conducting new experiments.

Finally, note that the present review constitutes a logical development of the recent reviews by Zhernov and Inyushkin [59], where, however, the main emphasis has been put on the dependence of thermal conductivity of crystals on the isotope composition in crystals with weak scattering potential relevant for isotope substitution. The latter circumstance allows an easy description of the observed effects in the framework of perturbation theory in harmonic approximation. In the present review we consider the influence of the isotope effect on elastic, thermal, and vibrational properties of various crystals, including the case of a strong phonon scattering potential relevant for isotope substitution, for a description of which, as will be shown, the harmonic approximation turns out to be insufficient.

2. Elastic properties

2.1 Theoretical foundations

The velocity of elastic wave v in a crystalline substance depends on its density ρ and the adiabatic elastic constant C_{ij}. The propagation velocities of the three modes can be calculated by solving the Kristoffel equation

$$\left|\Gamma_{ik} - \delta_{ik}\rho v^2\right| = 0\,, \tag{1}$$

where

$$\Gamma_{ik} = C_{ijkl}\,n_j\,n_l\,, \tag{2}$$

in which n_j are the directional cosines with respect to the direction of propagation (see, e.g., Ref. [60]). It is known [61] that substances having cubic symmetry have three independent elastic constants. For each $\langle 100\rangle$ direction the solutions of (1) can be written in the following form:

$$v_1 = \left(\frac{C_{11}}{\rho}\right)^{1/2}, \tag{3}$$

$$v_2 = v_3 = \left(\frac{C_{44}}{\rho}\right)^{1/2}, \tag{4}$$

where v_1 is the velocity of the longitudinal wave and v_2 is that of the transverse one. For the $\langle 100\rangle$ direction we obtain from (2)

$$v_4 = \left[\frac{1}{2}(C_{11} + C_{12}) + C_{44}\right]^{1/2}\rho^{-1/2}, \tag{5}$$

$$v_5 = \left(\frac{C_{44}}{\rho}\right)^{1/2}, \tag{6}$$

$$v_6 = \left(\frac{C_{11} - C_{12}}{\rho}\right)^{1/2}. \tag{7}$$

In these expressions v_4 is the velocity of the longitudinal wave, v_5 is the velocity of the transverse wave with particles moving in the $\langle 001\rangle$ direction, and v_6 is the velocity of the transverse wave with particles moving in the $\langle 110\rangle$ direction.

Choosing an appropriate crystal orientation and a set of measured sound velocities and using Eqns (3)–(7), one can calculate the elastic constants C_{11}, C_{12}, and C_{44}. For most directions in the crystal, Eqn (1) does not provide a simple relation between the elastic constants and the corresponding velocities. However, as shown in Ref. [62], it is possible to determine the elastic constants from measured velocities of ultrasound propagating in an appropriate direction by using the method exploiting perturbation theory. The authors of Ref. [63] used this method in estimating the elastic constants of TlCl crystal, where it was possible to use Eqns (3)–(7), because the $\langle 100\rangle$ and $\langle 110\rangle$ planes could not be obtained with sufficient accuracy. Later this method was used in determining the elastic constants of LiH and its isotope analogue LiD [64].

Another method of determining elastic constants in solids is the Mandelstam–Brillouin light-scattering method. It has got wide coverage in the literature (see, e.g., [65–67]). Here it is reasonable to remind the reader that for materials having a cubic structure the phonon quasi-momentum conservation law in the case of Mandelstam–Brillouin scattering takes the form

$$\mathbf{q} = \pm(\mathbf{k}_\mathrm{i} - \mathbf{k}_\mathrm{s}), \quad |\mathbf{q}| = \pm 2|\mathbf{k}_\mathrm{i}|\sin\frac{\theta}{2}\,, \tag{8}$$

where $\mathbf{q}$, $\mathbf{k}_\mathrm{i}$, and $\mathbf{k}_\mathrm{s}$ are the wave vectors of the phonon, the incident and the scattered light, respectively, and θ is the angle between $\mathbf{k}_\mathrm{i}$ and $\mathbf{k}_\mathrm{s}$. Note that $\mathbf{k}_{\mathrm{i,s}}$ and θ are determined inside the material and, therefore, in this case the effects related to the refracting crystal surfaces are not taken into account.

In an isotropic medium the velocity of an elastic wave v is calculated from the frequency shift $\delta\nu$ of the Mandelstam–Brillouin scattering line using the following relation:

$$\frac{\delta\nu}{\nu_0} = 2n\,\frac{v}{c}\sin\frac{\theta}{2}\,, \tag{9}$$

where c is the speed of light, n is the refractive index for the radiation frequency ν_0, θ is the scattering angle inside the crystal, and $\delta\nu$ is the frequency shift of the scattering line (for more details see Ref. [66]).

2.2 Experimental results

2.2.1 LiH crystals. The low-temperature values of C_{11} and C_{44} have been determined in Ref. [64] by measuring the velocities of longitudinal and transverse waves propagating in the $\langle 100\rangle$ direction. The authors have measured the sound propagation time and, using equations (3) and (4) and taking into consideration the size, density, and thermal expansion of the specimen, have found C_{ik}. According to [68, 69], at room temperature the densities of LiH and LiD are equal to 783 and 891 kg m^{-3}, respectively. Considering the errors arising in measuring the specimen length, propagation time, and density, the above-mentioned authors give for C_{12} an absolute error of $\sim$5%, whereas the error in determining C_{11} and C_{44} is much smaller (for more details see Ref. [70]).

At room temperature the elastic constants of ^{7}LiH and ^{7}LiD crystals have been measured in [68, 71], and for the LiH crystal in [69]. The values of elastic constants obtained by different authors for lithium hydride and lithium deuteride crystals are given in Table 1.

Table 1. Values of elastic constants in ^{7}LiH (C^1_{ij}) and ^{7}LiD (C^2_{ij}) (all in GN m^{-2}).

C^1_{11}	C^1_{12}	C^1_{44}	δC_theor	δC_exper	B^1_s, 10^{-11} dyn s^{-1} m^{-2}	C^2_{11}	C^2_{12}	C^2_{44}	B^2_s, 10^{-11} dyn s^{-1} m^{-2}	References
65.31 ± 0.2	14.85 ± 0.3	45 ± 1.1				66.26 ± 2	14.63 ± 0.3	45.53 ± 1.8		[71]
67.1 ± 0.3	14.9 ± 0.3	46.0 ± 0.2			32.0	67.8 ± 0.2	14.2 ± 0.2	47.8 ± 0.2	31.7	[68]
67.2 ± 1.3	14.93 ± 2.3	46.37 ± 1.6			32.4				33.5	[69]
67.1 ± 0.7	17.5 ± 3.5	46.0 ± 0.5								[90]
67.49 ± 0.33	14.74 ± 0.74	46.2 ± 0.23	1.8	2.2–3.4	34.2 (10 K)				35.6 (10 K)	[64]

We see that the results for ^{7}LiH are in good agreement. It is necessary to mention an essential disagreement in the value of C_{12}. The reasons for this are not quite clear. The results in Table 1 show a large distinction in the values of the constants C_{11} and C_{44} in LiH and LiD. It is well known [72] that for crystals with an inversion center, in the model of central forces, the Cauchy rule $C_{11} = C_{44}$ should hold. In microscopic description of lattice dynamics the Cauchy rule follows from the spherical distribution of ionic charges. This rule holds for quite a few ionic crystals. The biggest deviation from the Cauchy rule is observed in LiF, where $C_{11}/C_{44} = 1.53$, and the effective Szigetti charge $e_S^* = 0.8$ (see, e.g., Ref. [55]). As is seen from Table 1, this ratio for LiH (LiD) exceeds 3. This means that noncentral forces play an important role (see also Ref. [73]). The essence of the isotope effect reveals itself in the values of C_{11} and C_{44}, in LiD being larger than those in LiH, while the opposite statement is true for C_{12}. Note in passing that, according to direct calculations of the elastic constants in LiH [69], the value of C_{44} is strictly dependent on the allowance for interaction between the nearest neighbors in the next coordination shell.

In the low-temperature limit, the Debye temperature (Table 2) is determined from the relation that takes into account the velocities of the longitudinal and transverse waves (see, e.g., Ref. [70]):

$$\theta = \frac{\hbar}{k_B}\left(\frac{9N}{2V}\right)^{1/3}\left(\frac{1}{v_l^3}+\frac{1}{v_t^3}\right)^{-1/3}. \tag{10}$$

Analysis of the values of θ obtained in experiments on measuring the elastic constants and calorimetric measurements demonstrates good agreement [55] (see Section 3). It should be noted that for isotope substitution in LiH (D substituted for H), C_{ik} grows by 3%, and in diamond by 0.5% [79]. Such measurements of δC_{ik} are possible not only in ultrasound measurements, but in Mandelstam – Brillouin light-scattering as well.

2.2.2 Diamond crystals. Many of the properties of diamond are unique: the small atomic mass, the largest elastic constants, the fastest speed of sound and, certainly, high Debye temperature, attesting to, as in the case of LiH [55], quantum properties at room temperature (see also Ref. [57]). The dependence of diamond elastic constants on isotope composition has been studied in a number of papers [79 – 82]. The Mandelstam – Brillouin light-scattering method was used in [79, 81, 82] (Fig. 1), while in Ref. [80] the measurement of the elastic constants was made by the ultrasound method. Experiments on Mandelstam – Brillouin light scattering have been made in backscattering geometry for the vector $\mathbf{q}$ of the phonons propagating along the $\langle 001\rangle$, $\langle 111\rangle$ and $\langle 110\rangle$ directions. The laser light beam was perpendicularly incident on the surface of the specimens studied (see Fig. 3). In Ref. [81] a theory of determining the isotope dependence of the frequency of the limiting optical phonon $\hbar\omega_0$, the lattice parameter a, and the elastic constants C_{ik} has been given. The earlier developed lattice-dynamics theory for crystals with diamond structure [83 – 85] was based on the model that takes into account changes in the bond lengths and angles. The model of anharmonicity used in Ref. [84] included three harmonic and three anharmonic force constants. The authors of [81] have considered a simple model taking into account four parameters: two harmonic and two anharmonic. The harmonic part is analogous to the one already used in [60]. Following the authors of Ref. [81], we denote by $\Delta r_{i\mathbf{n}}$ the change in the distance between the central ion and its tetrahedral surroundings, and by $\Delta\theta_{ij\mathbf{n}}$ the change in the bond angle between two adjacent tetrahedral ions. The energy required for the increase Δr_i in the bond length equals

$$\frac{1}{2}k_1(\Delta r_i)^2 - \frac{1}{6}g_1(\Delta r_i)^3 + \ldots \tag{11}$$

To change the above-mentioned angle by $\Delta\theta_{ij\mathbf{n}}$, one needs an energy

$$\frac{1}{2}k_2(R\Delta\theta_{ij})^2 - \frac{1}{6}g_2(R\Delta\theta_{ij})^3 + \ldots \tag{12}$$

Here, k_1 and k_2 are the force constants in the harmonic part of the potential, whereas g_1 and g_2 determine, in the lowest order

Table 2. Thermal and dielectric characteristics of lithium hydride , lithium deuteride, and diamond.

Substance	θ, K	ε_0	ε_∞	$\alpha_T \times 10^6$, K^{-1}	e_S^*/e	ω_{TO}, cm^{-1}	ω_{LO}, cm^{-1}
LiH	860 [74] 1190 ± 80 (T = 0 K) [75] 1080 (T = 300 K) [75] 1083 (T = 300 K) [68] 1135 [69]	12.9 ± 0.5 [55]	3.61 [55]	36.5 (T = 300 K) [55]	0.53 ± 0.02 [55]	592 [55]	1120 ± 10 1109 (Li^{7}H) [55] 1129 (Li^{6}H) [55]
LiD	1030 ± 50 (T = 0 K) [75] 905 (T = 300 K) [68] 1032 (T = 300 K) [68]	14.0 ± 0.5 [64]	3.63 [55]	41.4 (T = 300 K) [55]	0.56 ± 0.02 [55]	444 [66]	880 ± 9 [55] 837 [76]
^{12}C	1860 (T = 300 K) [77, 78] 2200 (T = 300 K) [79]						1280 [77]
^{13}C	2114 (T = 300 K) [78]						1332 [79]

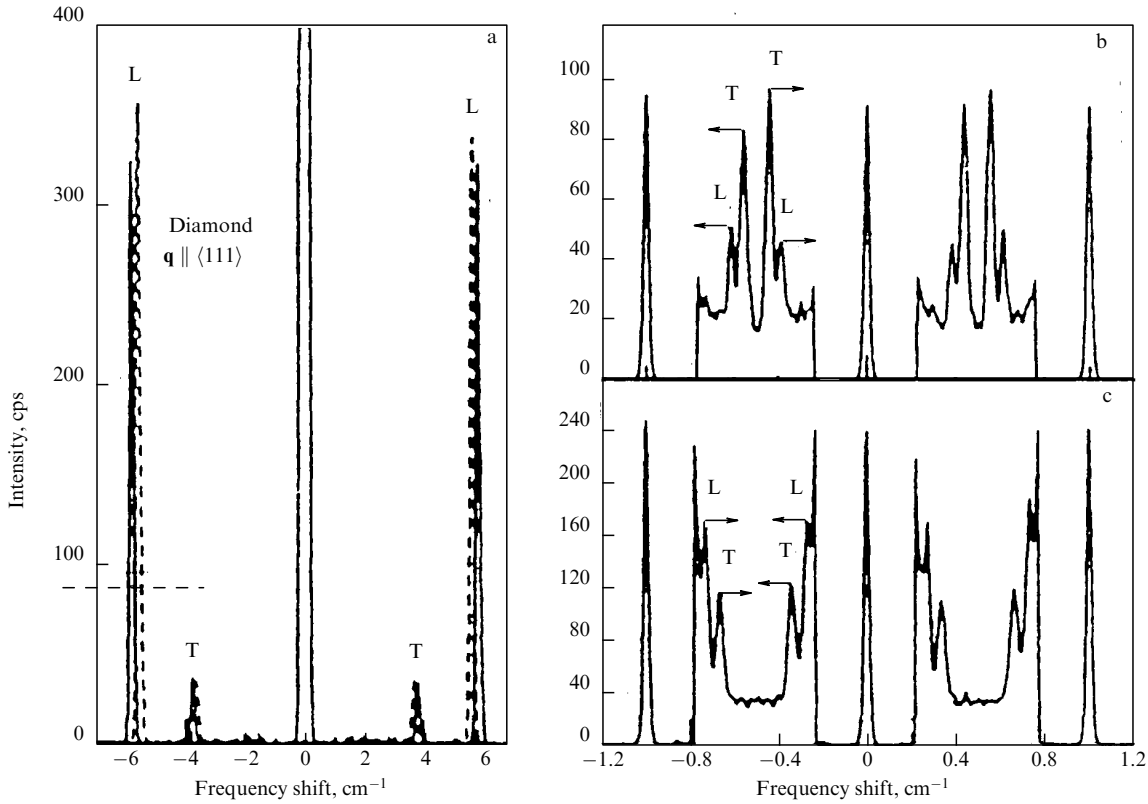

Figure 1. Mandelstam – Brillouin light-scattering spectra of (—) natural and (- - -) isotopically enriched ^{13}C diamond: (a) the spectra measured in the backscattering geometry for $\lambda_L = 5145$ Å and laser beam excitation along the ⟨111⟩ direction. The scattered light was analyzed by a (5+4) tandem of Fabry – Perot interferometers. L and T denote the longitudinal and transverse waves respectively; (b) Mandelstam – Brillouin spectrum for ^{13}C in the same geometry as in Fig. 1a, but with the spectrum analyzed by a five-way Fabry – Perot interferometer. The intensity of the longitudinal L and transverse T wave peaks is approximately 8.4 and 5.4 orders of magnitude less than the intensity of the exciting laser line; and (c) same as in Fig. 2b, but for ^{12}C. The intensity of L and T peaks is now 8.7 and 5.7 orders of magnitude less than that of the exciting laser line [81].

in perturbation theory, the anharmonic contributions. Taking into account only the interaction between the nearest neighbors, we have for the deformation energy

$$\Delta U = \sum_{\mathbf{n}} \Delta U_{\mathbf{n}} = \sum_{\mathbf{n}} \left[\frac{1}{2} k_1 \sum_i (\Delta r_{i\mathbf{n}})^2 + \frac{1}{2} k_2 \sum_{i<j} (R\Delta\theta_{ij\mathbf{n}})^2 - \frac{1}{6} g_1 \sum_i (\Delta r_{i\mathbf{n}})^3 - \frac{1}{6} g_2 \sum_{i<j} (R\Delta\theta_{ij\mathbf{n}})^3 + \dots \right]. \quad (13)$$

Elastic modulus. The energy required for deformation that does not change the symmetry and changes the distance from R to $R+u$ ($u \ll R$), i.e., $\Delta r_{i\mathbf{n}} = u$ and $\Delta\theta_{ij\mathbf{n}} = 0$, is written as

$$\Delta U = N\left(2k_1 u^2 - \frac{2}{3} g_1 u^3 + \dots\right), \quad (14)$$

where N is the number of primitive cells in the crystal.

The change in volume is equal to $\Delta V = 3Vu/R$, so that

$$\Delta U = \frac{k_1 (\Delta V)^2}{6aV} - \frac{g_1 (\Delta V)^3}{72\sqrt{3}\, V^2} + \dots \quad (15)$$

The dependence of the free energy on volume is expressed by the following equation:

$$\Delta F = \frac{1}{2} (\Delta V)^2 \left(\frac{\partial^2 F}{\partial V^2}\right)_0 + \dots \approx \frac{(\Delta V)^2 B}{2V}, \quad (16)$$

where B is the volume modulus. Comparison of (15) and (16) at $T = 0$ K gives

$$B = \frac{k_1}{3a}. \quad (17)$$

Energy of the limiting optical phonon $\hbar\omega_0$. When two face-centered sublattices move against each other along the ⟨111⟩ direction, the term g_2 exactly cancels, so that the deformation energy for this relative shift is

$$\Delta U = N\left[\frac{2}{3}(k_1 + 4k_2)\, u^2 - \frac{4g_1 u^2}{27} + \dots\right]. \quad (18)$$

In this relative motion, the kinetic energy corresponding to one primitive cell is equal to P^2/M, where P is the momentum canonically conjugate to u, and M is the mass of the atom ($M/2$ is the reduced mass in the case of diamond). Then the Hamiltonian corresponding, for this motion, to the primitive cell, is

$$H = \frac{P^2}{2M} + \frac{2}{3}(k_1 + 4k_2)\, u^2 - \frac{4g_1 u^3}{27} + \dots \quad (19)$$

In harmonic approximation, the angular frequency of the optical phonon F_{2g} in the center of the Brillouin zone ($\Omega_0 = \hbar\omega_0$) equals

$$\Omega_0 = -\left[\frac{8(k_1 + 4k_2)}{3M}\right]^{1/2}. \quad (20)$$

In order to estimate the effect of zero vibrations, in the cited paper [81] the Hamiltonian (19) has been quantized. Choosing, following [81], the normalized wave function in the form

$$\Psi(u) = \left(\frac{\alpha}{\sqrt{\pi}}\right)^{1/2} \exp\left[-\frac{\alpha^2}{2}(u-\delta)^2\right], \tag{21}$$

where α and δ are the variational parameters, one can calculate the value of the Hamiltonian H in the state $\Psi(u)$

$$E(\alpha,\delta) = \frac{\hbar^2\alpha^2}{2M} + \frac{2}{3}(k_1+4k_2)\left(\delta^2+\frac{1}{2\alpha^2}\right) - \frac{4g_1}{27}\left(\delta^3+\frac{3\delta}{2\alpha^2}\right)+\ldots \tag{22}$$

For a given δ, the minimum of $E(\alpha,\delta)$ corresponds to the following value of α:

$$\alpha = \left(\frac{M\Omega_0}{2\hbar}\right)^{1/2}\left(1-\frac{16g_1\delta}{9M\Omega_0^2}\right)^{1/4}. \tag{23}$$

Then,

$$E(\delta) = \frac{\hbar\Omega_0}{2} + \frac{1}{4}M\omega_0^2\left(\delta-\frac{8\hbar g_1}{9M^2\Omega_0^3}\right)^2 - \frac{16\hbar^2 g_1^2}{81M^3\Omega_0^4}+\ldots \tag{24}$$

with

$$\omega_0 = \Omega_0\left(1-\frac{32\hbar g_1^2}{81M^3\Omega_0^5}\right). \tag{25}$$

We see that the minimum of the total energy corresponds to a displacement $\delta = 8\hbar g_1/9M^2\Omega_0^3$ with respect to the classical value obtained by neglecting the kinetic energy due to zero vibrations of the atoms. The latter effect results in the renormalization of the optical phonon frequency according to formula (25).

Let us now briefly discuss the impact of zero vibrations on the magnitude of the volume modulus B. To this end, let us consider the homogeneous expansion of a crystal without changing its symmetry but taking into account the effect of zero vibrations. Let us use a procedure analogous to the one considered above used for the renormalization of ω_0. For a homogeneous change in volume, the Hamiltonian of the primitive cell reads

$$H = \frac{P^2}{M} + 2k_1u^2 - \frac{2}{3}g_1u^3+\ldots \tag{26}$$

Using the variational wave function as in (21) and minimizing the average value of the Hamiltonian (26) with respect to α, we obtain

$$E(\delta) = \hbar\left(\frac{2k_1}{M}\right)^{1/2} + 2K_1(\delta-\delta_0)+\ldots, \tag{27}$$

where K_1 determines the renormalized stiffness constant

$$K_1 = k_1\left[1-\frac{\hbar g_1^2}{8\sqrt{2}\,k_1^{5/2}M^{1/2}}\right], \tag{28}$$

$$\delta_0 = \frac{\hbar g_1\sqrt{2}}{8k_1^{3/2}M^{1/2}}. \tag{29}$$

As a result, the renormalized volume modulus T is described by the following relation:

$$T = \frac{K_1}{3a}. \tag{30}$$

Taking into account the effect of zero vibrations on the lattice parameter, we have

$$a_0 = a_\infty + \frac{\hbar g_1}{\sqrt{6}\,k_1^{3/2}M^{1/2}}, \tag{31}$$

where a_∞ is the distance between the nearest neighbors in the case of the infinite mass of the atoms and when zero vibrations are neglected. Simultaneously taking into account the dependences of the lattice parameter $a(x)$ and the frequency of the limiting optical phonon $\omega_0(x)$ on the energy of zero vibrations and the anharmonicity, we have

$$a(x) = a(0) - \frac{\hbar g_1}{(6k_1^3M_0)^{1/2}}\left[1-\left(\frac{M_0}{M_x}\right)^{1/2}\right],$$

$$\omega(x) = \omega(0)\left(\frac{M_0}{M_x}\right)^{1/2}\left\{1+\frac{32\hbar g_1^2}{81M_0^3\omega(0)^5}\left[1-\left(\frac{M_0}{M_x}\right)^{1/2}\right]\right\}.$$

The values of the elastic constants have been determined from the experimental results of Ref. [81] (Table 3). The elastic constants X were calculated from the formula

$$X(x) = \frac{C^2\rho(x)}{4\omega_L^2 n^2(x)}\Delta\omega^2(x), \tag{32}$$

where the density of ^{13}C depends on the isotope concentration x as follows:

$$\rho(x) = \frac{8M_x}{a^3(x)}, \quad \Delta\omega = \pm 2\omega_L\, n\,\frac{V_s}{c}\sin\frac{\theta}{2},$$

and $a(x)$ was determined, following Ref. [86], from the formula

$$a(x) = 3.56715 - 0.00053x. \tag{33}$$

The thus-found value of $\rho(x) = 3.5152$ g cm^{-3} is, taking into account (33), comparable with the value of density 3.5153 g cm^{-3} mentioned in Ref. [87]. In Ref. [81] the values of C_{11}, C_{12}, and C_{44} for three concentrations of x equal to 0.0, 0.01105, and 0.992 have also been found (see Table 3). In the last formulas, ω_L is the frequency of the laser radiation, n is the refractive index of the scattering medium (in our case, diamond), V_s is the speed of sound, and c is the speed of light in a vacuum.

A theoretical estimate for $T(x)$ has been given by the following expression:

$$\frac{T(x)}{T(0)} = \frac{a(0)}{a(x)}\left\{1+\frac{\hbar g_1^2}{8(2k_1^5M_0)^{1/2}}\left[1-\left(\frac{M_0}{M_x}\right)^{1/2}\right]\right\} = 1+0.0012x, \tag{34}$$

Table 3. Elastic constants C_{ij} and the volume modulus T in units of 10^{12} dyn cm^{-2} in diamond [81].

x	Sample	C_{11}	C_{12}	C_{44}	T
0.0	D29	10.799(5)	1.248(10)	5.783(5)	4.432(8)
0.01105	D1. D2. D17	10.804(5)	1.270(10)	5.766(5)	4.448(8)
0.992	D30	10.792(7)	1.248(14)	5.776(7)	4.429(12)

where for diamond $k_1 = 4.76 \times 10^5$ dyn cm^{-1} and $g_1 = (4.5 \pm 0.4) \times 10^{14}$ erg cm^{-3}.

The third-order elasticity modulus T' can be expressed through the parameter of anharmonicity g_1:

$$T' = \frac{dT}{dP} = \frac{V}{T}\,\frac{\partial T}{\partial g_1}\,\frac{\partial V}{\partial g_1} = \frac{g_1}{12\sqrt{3}\,T} = \frac{g_1 a}{4\sqrt{3}\,k_1} = 4.9\,. \quad (35)$$

Assuming further that the volume modulus is linearly dependent on pressure, one can obtain the Mungham equation of state

$$\frac{V_0}{V} = \left(1 + p\,\frac{T_0'}{T_0}\right)^{1/T_0'}, \quad (36)$$

where T_0' is the derivative of the volume modulus with respect to pressure estimated at $P = 0$. The experimentally derived value of T_0' [82] equals 4.03, so that it can be concluded that the molar volume of ^{12}C equals that of ^{13}C under a pressure of $P = 0.2$ GPa. One has, therefore,

$$\frac{T(^{13}\mathrm{C}) - T(^{12}\mathrm{C})}{T(^{12}\mathrm{C})} = 1.8 \times 10^{-3}\,. \quad (37)$$

This estimate is in reasonable agreement with the previous value obtained from formula (34). An analysis of the contradictory results of the ultrasound measurements of the elastic constants in diamond [80] can be found in reference [70]. Based on the results of the experiment on LiH and LiD in Ref. [88], a value $g_1 = 3.5 \times 10^{15}$ erg cm^{-3} has been obtained. It is easy to see that by substituting equation (28) into expression (32) one can find the relation describing the renormalization of elastic constants due to the isotope effect (see also Ref. [70]),

$$\Delta C_{44} = \frac{k_1}{8a}\left[1 - \left(\frac{\hbar g_1}{8K^2}\right)^2 \frac{1}{\sqrt{K\mu}}\right], \quad (38)$$

where μ is the reduced mass of the primitive cell. According to the experimental data of Ref. [69], the relative change δC_{44} after isotopic substitution in lithium hydride is equal to 2.2–3.4%, whereas the estimate of (37) gives a value of 1.8% [88]. In the last paper it is mentioned that the difference between the theory and experiment can be explained even by taking into account only the lowest order anharmonicity that was used in this paper (see also Ref. [89]).

2.3 Temperature dependence of elastic constants

Temperature dependence of elastic constants in LiH and LiD crystals has been studied by both the ultrasound method [64, 68, 69] (Fig. 2) and the Mandelstam–Brillouin light-scattering method [74, 90] in a temperature interval of 4.2–300 K. It has been shown that the constants C_{11} and C_{44} grow with decreasing temperature, whereas C_{12} diminishes. The weak dependence of the volume modulus on temperature is explained by the partial cancellation of C_{11} and C_{12} contributions (see also Refs [91–96]).

The authors of Ref. [52] have shown that the temperature dependence of the elastic constants can be described as follows:

$$C_{ij}(T) = C_{ij}(0)\,(1 - D\bar{\varepsilon})\,, \quad (39)$$

where D is the parameter depending either on the type of the crystal or on the model, and $\bar{\varepsilon}$ is the energy of a single

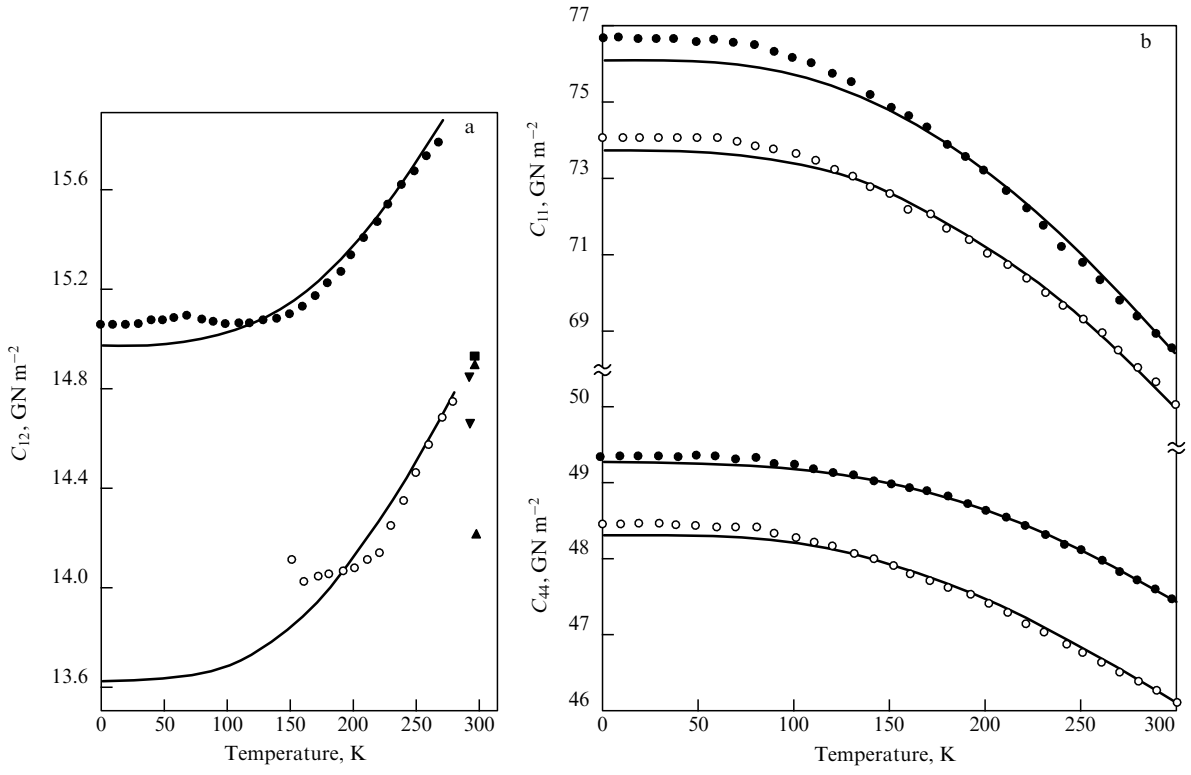

Figure 2. (a) Temperature dependence of the elastic constant C_{12} of (○) ^{7}LiH and (●) ^{7}LiD crystals [64]; and (b) temperature dependence of the elastic constants C_{11} and C_{14} in (○) ^{7}LiH and (●) ^{7}LiD crystals. The solid lines show the results of calculations according to formula (39) [64].

oscillator. When using the Debye – Einstein model, the above expression gives a sufficiently good description of the temperature dependence of the elastic constants. Using this particular method, in Ref. [64] a reasonably good agreement between theory and experiment for the crystal of lithium hydride and its isotopic analogue has been obtained [97 – 101].

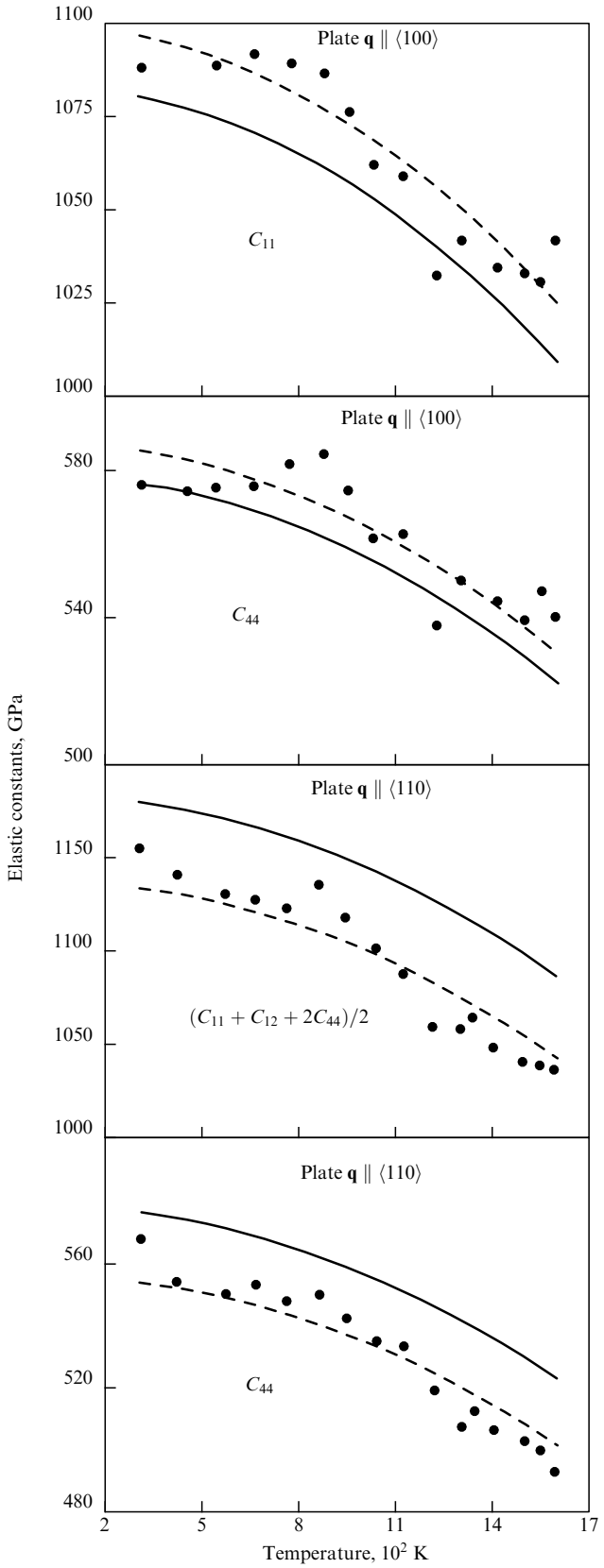

Figure 3. Temperature dependences of the elastic constants of diamond obtained in different crystallographic directions and in the 90° scattering geometry: (——) calculation according to formula (40), (– – –) calculation using the improved model of Ref. [82], and (•) experimental points.

The temperature dependence of the elastic constants in diamond has been studied by the Mandelstam – Brillouin light-scattering method in Ref. [82]. For a theoretical description of the elastic constants of diamond, the authors have used a polynomial of the following form:

$$C_{ij}(T) = C_0 + C_1(T - 300) + C_2(T^2 + 300^2)\,. \qquad (40)$$

To describe the elastic constants of diamond, it has been necessary to use nine free parameters C_0, C_1, and C_2 (Fig. 3). As a result, the following values of the elastic constants at room temperature have been obtained: $C_{11} = 1080.4$ GPa, $C_{12} = 127.0$ GPa, and $C_{44} = 576.6$ GPa. The authors of Ref. [82] have described the temperature dependence of the volume modulus by the following expression:

$$B(T) = 444.8 - 0.000012(T^2 - 300^2)\,. \qquad (41)$$

The authors of the cited works have demonstrated that, after heating from room temperature to $T = 1600$ K, the diamond hardness diminished by 7 – 9 %.

Studies of the temperature dependence of elastic constants [82, 90] have allowed us to estimate the temperature dependences of force constants at the atomic level. Calculations of the force constants are done using either the model of Ref. [84] or that of Ref. [83]. In spite of the assumptions in these two models being the same, the physical results are, nevertheless, different. The first model [84] has two parameters, α and β, related to the zones of the stretching and bending vibrations, whereas the second one [83] comprises four force constants. The authors of [82] have used two constants k_1 and k_2, describing, correspondingly, the stretching and bending vibrations (for more details see Ref. [70]).

3. Thermal properties

3.1 Dependence of the thermal conductivity of diamond, germanium, and silicon on isotope composition

Thermal conductivity of crystals has been a subject of many experimental and theoretical studies (see, e.g., reviews and monographs [102 – 105]). The first experimental results (see, e.g., [106]) have already pointed out the existence of maximum of the thermal conductivity coefficient k_m at about $T \approx 0.05\theta_D$, where θ_D is the Debye temperature (Fig. 4). The growth of k at low temperatures has been related to phonon scattering due to Umklapp-type processes (see also Ref. [107]). In the vicinity of k_m, thermal conductivity is quite sensitive to impurities and defects in the specimen. In the usual models, the thermal conductivity of insulators, in which the carriers are scattered only by phonons, is described by the thermal conductivity equation in the relaxation-time approximation (see Refs [53, 102]).

3.1.1 Theoretical models. In this paragraph we give a brief description of the main theoretical models used in the analysis of experimental data on thermal conductivity [102, 106, 108]. Klemens [102] has obtained the phonon scattering rate (analogous to the Rayleigh photon scatter-

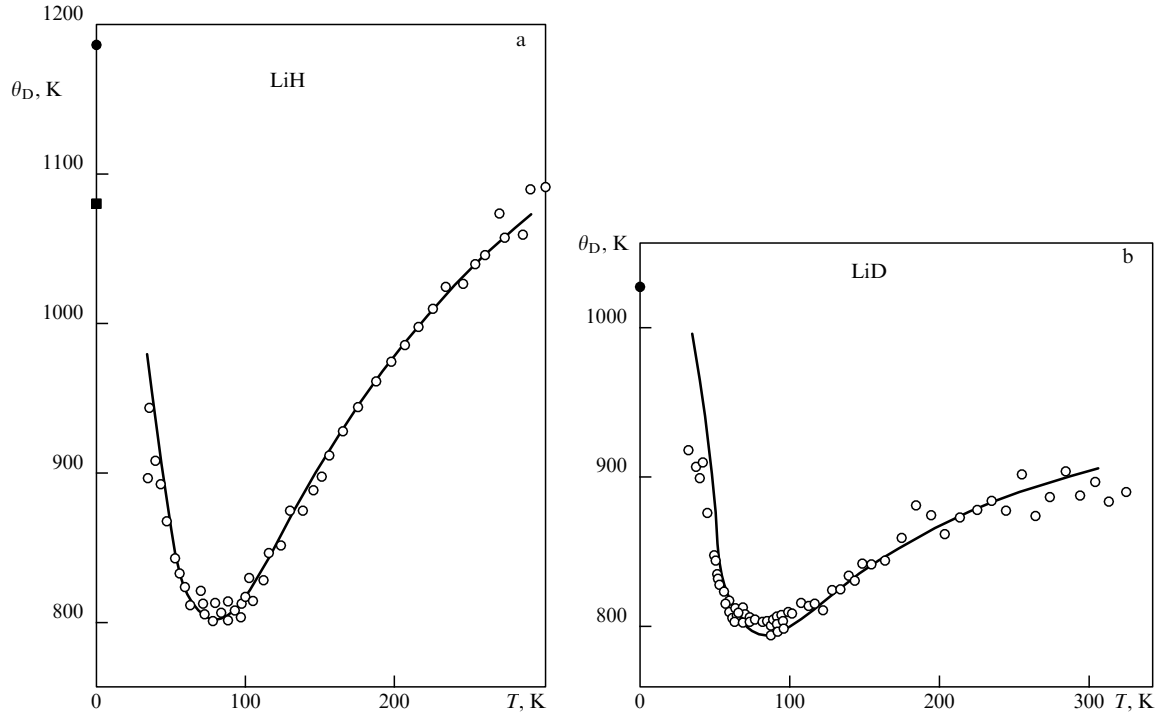

Figure 4. Temperature dependence of the Debye temperature of (a) LiH and (b) LiD crystals [98].

ing) equal to

$$\tau^{-1} = A\omega^4 , \tag{42}$$

$$A = \frac{gV}{4\pi v_B^3} . \tag{43}$$

Here, the constant A describes the change in the mass,

$$g = \frac{\sum c_i M_i^2 - \left(\sum c_i M_i\right)^2}{\left(\sum c_i M_i\right)^2} , \tag{44}$$

where c_i and M_i are the concentration and the isotope mass, respectively. The mean free path calculated by Klemens was defined as $L_i \sim gT^4$, where g is a quantity describing the isotope change of the mass. In formulas (42) and (43), V denotes the atomic volume and v_B the mean sound velocity. Equation (42) corresponds to the Debye-like density of states $D(\omega) \sim \omega^2$ which, as will be seen below, is taken into account in explaining the experimental results.

At low temperatures and for phonon scattering by crystal boundaries, the thermal conductivity behaves as $k \sim T^3$ with a prefactor being determined by both the specimen geometry and the details of the surface. The scattering rate can be written as follows:

$$\tau^{-1} = \frac{v_B}{L_E} , \tag{45}$$

where L_E is the effective phonon mean free path, which depends on many factors (specimen geometry, phonon focusing, mirror (diffuse) reflection from the surface, etc.).

Below, a brief account of the widely used $k(T)$ scattering theory that was formulated by Callaway [109] and of its modifications introduced by Holland [103] is presented.

The Callaway model. According to this model

(1) one assumes a Debye-like phonon spectrum not having any structure, with no account for any type of anisotropy or phonon polarization (indistinguishibility of transverse and longitudinal phonons);

(2) only the mean sound velocity v_B is considered;

(3) the scattering by the surface is assumed to be exclusively diffusive [see equation (45)];

(4) the normal three-phonon processes, having relaxation times $\tau_N^{-1} = B_2\omega^2 T^3$, operate only for low-frequency longitudinal phonons;

(5) the relaxation time of the Umklapp processes is described analogously to that of the normal processes, $\tau_U^{-1} = B_1\omega^2 T^3$ (see also Ref. [102]);

(6) the relaxation times of all scattering processes are described separately;

(7) the relaxation times of various scattering processes are considered to be additive.

Within these assumptions, the full thermal conductivity takes the form (see also [110])

$$k = k_1 + k_2 , \tag{46}$$

where k_1 and k_2 are defined as follows:

$$k_1 = cT^3 \int_0^{\theta/T} \tau_C(x)\, J(x)\, dx , \tag{47}$$

$$k_2 = cT^3 \frac{\left\{\int_0^{\theta/T} \left[\tau_C(x)/\tau_N(x)\right] J(x)\, dx\right\}^2}{\int_0^{\theta/T} \left[\tau_C(x)/\tau_N(x)\,\tau_R(x)\right] J(x)\, dx} = cT^3(\beta I) . \tag{48}$$

Here,

$$\beta = \frac{\int_0^{\theta/T} \left[\tau_C(x)/\tau_N(x)\right] J(x)\, dx}{\int_0^{\theta/T} \left[\tau_C(x)/\tau_N(x)\,\tau_R(x)\right] J(x)\, dx} ,$$

$$I = \int_0^{\theta/T} \frac{\tau_C(x)}{\tau_N(x)} J(x)\, dx , \tag{49}$$

and

$$J(x)=\frac{x^4\exp x}{(\exp x-1)^2}\,,\quad \frac{1}{\tau_{\rm C}(x)}=\frac{1}{\tau_{\rm N}(x)}+\frac{1}{\tau_{\rm R}(x)}\,,$$
$$x=\frac{\hbar\omega}{k_{\rm B}T}\,,\quad m=\frac{k_{\rm B}}{\hbar}\,,\quad c=\frac{k_{\rm B}m^3}{2\pi^2 v_{\rm B}}\,. \tag{50}$$

In formula (50), $k_{\rm B}$ is the Boltzmann constant, $\hbar$ is Planck's constant, and $\tau_{\rm N}$ ($\tau_{\rm R}$) is the relaxation time of the normal processes (resistive processes). As is seen from Eqn (50), relaxation rate $\tau_{\rm C}^{-1}$ is a sum of the normal, nonresistive (N) and resistive (R) processes. As opposed to the earlier Klemens [102] and Ziman [108] models, in the Callaway formulation the probabilities of all resistive processes are additive, i.e., $1/\tau_{\rm R}=\sum_i(1/\tau_i)$ (where $\tau_{\rm i}$, $\tau_{\rm B}$, and $\tau_{\rm U}$ are the relaxation times corresponding to scattering by isotopes and crystal boundaries and due to Umklapp processes, respectively). From this, there follows that all corresponding phonon scattering mechanisms are assumed to be independent.

The term k_2 does not, as is sometimes assumed in the literature (see, e.g., Ref. [109]), constitute a correction to k_1, but is a normal counteraction to the effects of N-processes in $\tau_{\rm C}$ if they are all resistive. Therefore, k_2 is an integral part of the Callaway theory. Usually the quantity k_2 is determined by the concentration of point defects. In the main cases which present physical interest, resistive scattering dominates, $\tau_{\rm N}\gg\tau_{\rm R}\Rightarrow\tau_{\rm C}\approx\tau_{\rm R}\Rightarrow k_2\ll k_1$, and it is important to keep k_1 only. This is precisely for this reason that only the k_1 term is considered in the literature. However, when N-processes become comparable to the resistive ones ($\tau_{\rm N}\approx\tau_{\rm R}$), for example in a very pure, monoisotopic specimen, the integrals determining k_2 (48) make a sizeable contribution to thermal conductivity [110]. Therefore, in monoisotopic specimens, the normal three-phonon processes determine the phonon mean free path to a larger extent than the Umklapp ones.

The Holland model. The Holland theory constitutes the next step as compared to the Callaway theory because it explicitly includes both kinds of phonons, longitudinal and transverse. It is assumed that $k_2=0$. Because the changes in relaxation times with changing frequency and temperature are strictly determined by the types of the branches of phonons participating in the process and by their dispersions, the contributions to the thermal conductivity from the two types of phonons (longitudinal and transverse) are essentially different, although the normal processes are taken into account through the structure of the crystals considered, as earlier assumed in the paper by Herring [111].

Consideration of the transverse phonons in Ge, which has a large dispersion [112], is the most realistic. This leads to the division of the integration domain into two subdomains, low- and high-frequency, having different temperature and frequency dependences.

The four scattering mechanisms (see Table 4) of phonons in the Callaway model have the following temperature and frequency dependences:

$$\tau_{\rm I}^{-1}=A\omega^4\,, \tag{51}$$

$$\tau_{\rm B}^{-1}=\frac{v_{\rm B}}{L_{\rm E}}\,, \tag{52}$$

$$\tau_{\rm TO}^{-1}=B_{\rm T}\omega T^4\quad\text{at}\quad 0\leqslant\omega<\omega_1\,, \tag{53}$$

$$\tau_{\rm LO}^{-1}=B_{\rm L}\omega^2 T^3\quad\text{at}\quad 0\leqslant\omega<\omega_3\,, \tag{54}$$

$$\tau_{\rm TU}^{-1}=\begin{cases}\dfrac{B_{\rm TU}\,\omega^2}{\sinh x} & \text{at } \omega_1\leqslant\omega\leqslant\omega_2\,,\\ 0 & \text{at } \omega<\omega_1,\end{cases} \tag{55}$$

where $x=(\hbar\omega/k_{\rm B}T)$, and the indices T(L) refer to the transverse (longitudinal) acoustic phonons. According to Holland, the integral k_1 (in the Callaway notation) accounts for separate contributions from TA and LA, described by the expressions for $k_{\rm T}$ and $k_{\rm L}$. The $k_{\rm T}$ term is split into two terms, corresponding to contributions of the N-processes ($k_{\rm TO}$) and U-processes ($k_{\rm TU}$):

$$k=k_{\rm T}+k_{\rm L}=k_{\rm TO}+k_{\rm TU}+k_{\rm L} \tag{56}$$

where

$$k_{\rm TO}=\frac{2}{3}\,H_{\rm TO}T^3\int_0^{\theta_1/T}\tau_{\rm C}^{\rm TO}(x)\,J(x)\,{\rm d}x\,, \tag{57}$$

$$k_{\rm TU}=\frac{2}{3}\,H_{\rm TU}T^3\int_0^{\theta_2/T}\tau_{\rm C}^{\rm TU}(x)\,J(x)\,{\rm d}x\,, \tag{58}$$

$$k_{\rm L}=\frac{1}{3}\,H_{\rm L}T^3\int_0^{\theta_3/T}\tau_{\rm C}^{\rm L}(x)\,J(x)\,{\rm d}x\,, \tag{59}$$

and

$$\tau_{\rm C}^{\rm TO}(x)=\left(\frac{v_{\rm B}}{L_{\rm E}}+Am^4x^4T^4+B_{\rm T}mxT^5\right)^{-1},$$
$$\tau_{\rm C}^{\rm TU}(x)=\left(\frac{v_{\rm B}}{L_{\rm E}}+Am^4x^4T^4+\frac{B_{\rm TU}m^2x^2T^2}{\sinh x}\right)^{-1},$$
$$\tau_{\rm C}^{\rm L}(x)=\left(\frac{v_{\rm B}}{L_{\rm E}}+Am^4x^4T^4+B_{\rm L}m^2x^2T^5\right)^{-1},$$
$$H_i=\frac{k_{\rm B}m^3}{2\pi v_i}\,,\quad m=\frac{k_{\rm B}}{\hbar}\,. \tag{60}$$

In each of the three integrals, the constant H_i includes the corresponding sound velocity v_i. It is necessary to stress that in equation (57) one neglects the U-processes, because their contribution below ω_1 (for $\theta_1=101$ K for Ge) is equal to zero. In equation (58) the term corresponding to N-processes is omitted because above ω_1 their contribution is relatively small. As follows from the quantitative check [113], these assumptions are justified (for more details see Ref. [59]).

3.2 Experimental results

Diamond. The role of isotopes as an additional channel of phonon scattering and their influence on thermal conductivity were first theoretically studied by Pomeranchuk in 1942 [114], and were experimentally studied using Ge in 1958 [115]. According to the results of the latter reference, for a Ge specimen (having 95.8% ^{74}Ge), a threefold growth of the thermal conductivity coefficient as compared to the specimen of germanium with normal isotope composition was observed. Later, the influence of isotopes on diamond thermal conductivity was studied many times [78, 116–120]. The first results on diamond thermal conductivity have already shown that approximately a 1% decrease in the concentration of ^{13}C isotope in natural diamond (from 1.108 to 0.07%) leads to a 50% increase in $k_{\rm m}$, where $k_{\rm m}$ is the thermal conductivity coefficient at the maximum of the corresponding curve.

As an example, in Fig. 5a, according to the results of Ref. [113], the temperature dependence of the thermal conductivity of two specimens of type IIA diamond is

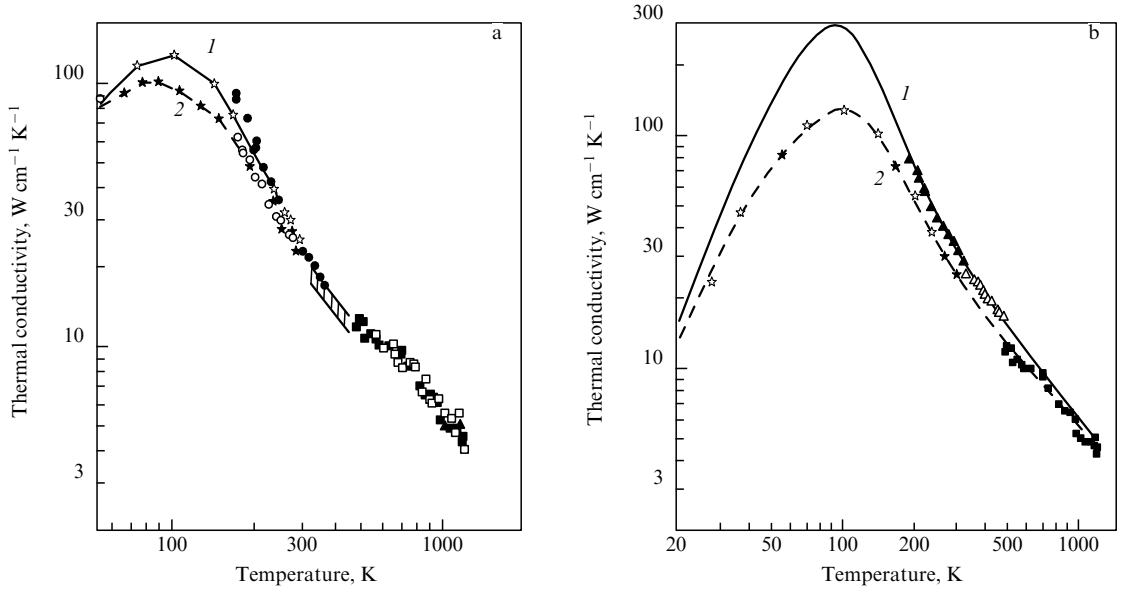

Figure 5. (a) Temperature dependences of the thermal conductivity of two type IIA diamond specimens [113]: (*1*) specimen No. 1 and (*2*) specimen No. 2; (b) temperature dependences of natural (type IIA) and synthetic diamonds with a ^{13}C concentration of 0.07%. The results of computations in the Debye model are shown by dashed line *2*. The solid line *1* describes the thermal conductivity of an almost monoisotopic (^{12}C) diamond, the Rayleigh term having served as a fitting parameter [113].

shown. The observed values of thermal conductivity agree well with those obtained earlier in the whole temperature interval. It is necessary to note, however, that a 10% difference in the values of thermal conductivity in the two specimens reflects, in the opinion of the cited authors, different concentrations of defects in the specimens studied. To describe the large growth of diamond thermal conductivity at a 1% drop in the concentration of ^{13}C isotope (Fig. 5b), the authors of Ref. [113] have used the Debye model

$$k(T) = Nk_B \sum_{i=1}^{3} v_i \left[\frac{T}{\theta_{D_i}}\right]^3 \int_0^{\theta_{D_i}/T} l(x)\, \frac{x^4 \exp x}{(\exp x - 1)^2}\, dx, \tag{61}$$

where N is the density of atoms (for diamond $N = 1.762 \times 10^{23}$ cm^{-3}), the summation over i includes one longitudinal and two transverse modes, v_i is the speed of sound, $v_l = 1.75 \times 10^6$ cm s^{-1} [120], $v_t = 1.28\times 10^6$ cm s^{-1}, and $\theta = \theta_{D_i}$ is the effective Debye temperature of the ith mode

$$\theta_{D_i} = 2.997 \times 10^{-11} v_i N^{1/3} sK. \tag{62}$$

Here, s is the number of vibrational branches, K is the combination of elastic constants (for more details see Refs [49, 53]), $l(x)$ is the mean free path, and

$$x = \frac{\hbar v_i}{k_B T \lambda}, \tag{63}$$

where λ is the phonon wavelength. As before [see formula (50)], it is assumed that the scattering velocity in the resistive processes is additive, i.e.,

$$l(x) = \left(l_{bound}^{-1} + l_{def}^{-1} + l_{Umkl}^{-1}\right)^{-1} + \frac{\lambda}{2}. \tag{64}$$

The terms l_{bound}, l_{def} and l_{Umkl} are the phonon mean free paths related to the boundaries of the specimen, point defects, and U-processes, respectively. The term $\lambda/2$ is included to avoid a nonphysical singularity in the case when the mean free path becomes comparable to the phonon wavelength.

In spite of the fact that in the literature the Debye model is often called the Klemens–Callaway model, the authors of Ref. [113] have chosen the former name. As is known, Klemens assumed that phonon scattering rates are additive and ignored N-processes, whereas Callaway took the latter into account.

It is necessary to note that in his analysis of experimental data [115] Callaway did not take into account N-processes and used a simple Debye model. According to Ref. [113], the mean free path is written as

$$l_{bound}^{-1} = \frac{1}{A}, \tag{65}$$

$$l_{def}^{-1} = \frac{B}{\lambda^4}, \tag{66}$$

$$l_{umkl}^{-1} = C\, \frac{T}{\lambda^2} \exp\left(-\frac{D}{T}\right). \tag{67}$$

Formulas (65) and (66) have already been used by Klemens [102] and Peierls [107]. A good agreement with experiment has been obtained [113] using the following values of parameters: $A = 0.1$ cm, $B = 4.0 \times 10^{-25}$ cm^3, $C = 2.0 \times 10^{-12}$ cm K^{-1}, and $D = 550$ K. The parameter values established are reproduced in Table 4. These values are quite close to those published earlier [78, 118, 120]. In reference [113] it was assumed that the scattering rate in N-processes is much larger than that in the resistive processes, both giving the same value of thermal conductivity in the Callaway and Ziman models, which is described by the following expression:

$$k(T) = Nk_B \sum_{i=1}^{3} v_i \left[\frac{T}{\theta_{D_i}}\right]^3 \times \frac{\left[\int_0^{\theta_{D_i}/T} x^4 \exp x (\exp x - 1)^{-2}\, dx\right]^2}{\int_0^{\theta_{D_i}/T} l^{-1}(x)\, x^4 \exp x (\exp x - 1)^{-2}\, dx}, \tag{68}$$

Table 4. Parameters of the Callaway and Debye models that describe the experiments on thermal conductivity of diamond [121].

Sample	A, cm	B, cm^3	C, cm K^{-1}	D, K
Debye model				
Natural diamond (type IIA)	0.1	4.0×10^{-25}	2.0×10^{-12}	550
Synthetic diamond (enriched with ^{12}C)	0.1	0.6×10^{-25}	2.0×10^{-12}	550
Callaway model				
Natural diamond (type IIA)	0.055	1.5×10^{-26}	1.4×10^{-12}	730
Synthetic diamond (enriched with ^{12}C)	0.055	0	1.4×10^{-12}	730

where $l^{-1}(x)$ is the inverse quantity of that determined by formula (64). In this case the parameters describing the experiment on thermal conductivity of diamond take the following values: $A = 0.055$ cm, $B = 1.5 \times 10^{-26}$ cm^3, $C = 1.4 \times 10^{-12}$ cm K^{-1}, and $D = 730$ K (Table 4, Callaway model). It is not surprising that these parameters differ from those found earlier in the framework of the Debye model. Thus, the observed influence of isotope scattering of phonons on the thermal conductivity of diamond is sufficiently well described by the modern theory taking into account the N-processes. At the same time one should add that the assumption of the dominance of N-processes leads to a disagreement between theory and experiment in describing the temperature dependence of thermal conductivity (see also [70]).

Germanium and silicon. Taking into account the high degree of purity ($|N_d - N_a| < 10^{14}$ cm^{-3}) and perfection of Ge specimens used in Ref. [121], we will mainly describe the experimental results obtained in this paper. Four phonon scattering mechanisms that determine the temperature dependence of thermal conductivity were considered:

(1) normal (N) three-phonon scattering processes,

(2) three-phonon processes,

(3) phonon scattering by the boundaries,

(4) isotopic (I) fluctuation of mass (point defects).

In Ref. [121] the parameters of the last two mechanisms were determined by the conditions of the theoretical model and have therefore been fixed. In that paper, the phonon scattering by dislocations has also been considered. The temperature dependence of the thermal conductivity of five Ge specimens with different isotope compositions is shown in Fig. 6a. The maximum value of $k_m = 10.5$ kW m^{-1} K^{-1} was observed, in the vicinity of $T = 16.5$ K, for the ^{70}Ge specimen of 99.99% purity, which is significantly higher than the value for sapphire (6 kW m^{-1} K^{-1} around $T_m = 35$ K) and comparable to the value for silver (11 kW m^{-1} K^{-1} near $T_m = 15.4$ K). The authors of Ref. [121] note that all specimens (with the exception of that containing 95.6% ^{70}Ge) had, within 10% accuracy, the same geometry. It can be seen that the thermal conductivity dependence is typical of dielectrics with a low concentration of defects — a T^3 law at low temperatures due to the scattering of phonons by the crystal boundaries and a maximum appearing due to the normal and Umklapp scattering processes and leading to $1/T$ dependence at $T > 100$ K. Comparison of experimental results shows (Fig. 6a) that, at its maximum, the thermal conductivity of the $^{70/76}$Ge (91.91%) specimen is 14 times less than that of ^{70}Ge (91.91 %). An increase in k reaches, however, only 30% at $T = 300$ K (see also Refs [59, 122]).

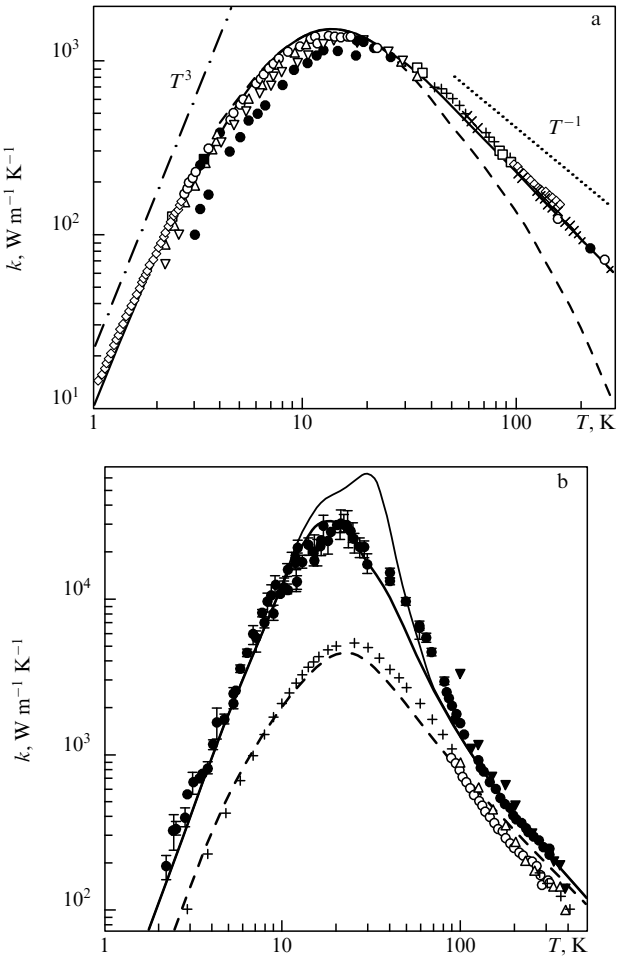

Figure 6. (a) Temperature dependence of thermal conductivity for five Ge specimens with different isotope composition: (– · –) the low-temperature T^3 law expected for phonon scattering by the boundary, (···) $1/T$ dependence expected for phonon scattering at high temperatures [121], and (– – –) calculation in the Callaway model; (b) thermal conductivity of highly enriched ^{28}Si crystals (the SI284 specimen, black circles) and natural Si crystal (SINI, open circles). Black and open triangles correspond to results for highly enriched ^{28}Si and natural Si obtained in Ref. [104]. The thin solid and dashed lines correspond to theoretical computation of thermal conductivity for monoisotopic ^{28}Si and natural Si specimens, respectively, performed in Ref. [124]. The thick solid line corresponds to the analogous theoretical computation of thermal conductivity of the SI284 specimen with the real value of $g_2 = 10^{-7}$ [125].

When using the Callaway model in its original form [see formulas (47), (48)], the two free parameters (B_1 and B_2) were chosen in combination with the four considered scattering mechanisms with a fixed rate of phonon scattering by isotopes and crystal boundaries. With these assumptions, the following parameter values have been obtained: $V = 22.6 \times 10^{-30}$ m^3; $v_B = 3500$ m s^{-1}; $0.01 \times 10^{-5} \leqslant g \leqslant 58.7 \times 10^{-5}$; $3.6 \leqslant L_E \leqslant 4.8$. It is appropriate to note that an agreement between the theory and experiment has been achieved only at $T \leqslant 30$ K. Analysis of experimental data has led the authors of [121] to the conclusion that in the framework of the Callaway model for monoisotopic specimens it is the normal three-phonon processes that are the main ones determining the phonon mean free path.

Let us now briefly discuss the experimental results of Ref. [121] obtained in the framework of the Holland model.

As already was mentioned, Holland was the first to explicitly include transverse and longitudinal phonons into consideration of thermal conductivity mechanism, assuming $k_2 = 0$. In the Holland model, the authors of [121] have used three fitting parameters B_T, B_L, and B_{TU}, equal to 1.1×10^{-11} K^{-4}, 6.9×10^{-24} s 5.0×10^{18} s K^{-4}, and 5.0×10^{18} s, respectively. Using the Holland model, the authors of [121] have obtained a good agreement between theory and experiment in the temperature range of 2 – 200 K (for more details see Refs [70, 121]).

The thermal conductivity of monoisotopic and isotopically mixed specimens of silicon crystals has been studied in three papers [123 – 125]. Since the most detailed results have been obtained by the authors of [125], we restrict ourselves to their consideration. It is well known that natural silicon consists of three isotopes: ^{28}Si ($\sim$92%), ^{29}Si ($\sim$5%), and ^{30}Si ($\sim$3%). The use of monoisotopic silicon (for example, ^{28}Si) can substantially reduce the value of dissipated energy scattered in electronic elements made of silicon (e.g., in the memory of electronic computers; see also Refs [32, 126]). The results of studies of the thermal conductivity of monoisotopic and isotopically mixed crystals are shown in Fig. 6b. According to the results presented in this figure, for the SI284 specimen $k = 237(8)$ W m^{-1} K^{-1} at 300 K, whereas for the SINI (natural Si) specimen it is equal to 150 W m^{-1} K^{-1}. This means that at 300 K the thermal conductivity of a monoisotopic ^{28}Si specimen grows, as compared to the natural silicon, by 60%. At the same time, at about 20 K (in the vicinity of the maximum of the silicon thermal conductivity curve) k reaches the value of 30000 ± 5000 W m^{-1} K^{-1}, which is 6 times higher than the value $k = 5140$ W m^{-1} K^{-1} for the natural specimen (see also Ref. [104]).

The thin solid and dashed lines in Fig. 6b correspond to the results of theoretical computations of thermal conductivity for a monoisotopic specimen SI284 and for a specimen with the natural silicon isotope composition. In these calculations, the model of the Ge thermal conductivity developed in [121] with a modified Debye temperature θ and phonon mean free path L_E has been used. For fitting, the authors have used the low-temperature results, where the thermal conductivity is described by the T^3 law. Calculations presented in Fig. 6b were performed, for the natural specimen, for $L_E = 5.0$ mm (dashed line). For comparison, let us point out that in Ref. [123] the analogous quantity was equal to $L_E = 5.7$ mm, and for the isotopically pure SI284 specimen the value was $L_E = 14.0$ mm (thin solid line). As seen from Fig. 6, there is agreement between theory and experiment, which has also been mentioned by the authors of Ref. [125] themselves. They have also pointed out good agreement between their experimental results and calculations made in Ref. [127], except for the domain of U-processes. Besides that, Ruf and co-authors have mentioned an unsatisfactory agreement between theory and experiment in the domain of high temperatures (300 – 400 K), especially for the specimen with natural isotope composition. They think that this disagreement can occur due to fundamental reasons that require further study. In particular, taking into account the fine structure of the nonequilibrium phonon distribution function could bring theoretical and experimental results much closer (see also Refs [59, 122, 128]). A qualitative comparison of the influence of the isotope effect on the thermal conductivity of germanium, silicon, and diamond is given in Table 5.

Table 5. Influence of isotope effect on the thermal conductivity of Ge, Si, and C specimens [118, 113, 121 – 125] at 300 K.

Sample	Growth of k, %	θ, K	g, 10^{-4}
Ge	30	376	5.80
Si	60	658	2.01
C	50	1868	0.76

Note. The concentration of other isotopes was determined by the relation $g = \sum_i f_i(\Delta M_i/M)$.

3.3 Influence of temperature and isotope composition on the lattice parameter

It is widely known that the lattice parameter is, at any temperature, determined by three factors. The first and the most important are the atomic radius and the nature of the chemical bond between the atoms. The latter determines not only the interatomic spacing, but also the crystal structure. The second contribution to a is due to the influence of temperature on the interatomic distance. As a rule, an increase in temperature leads to the expansion of the crystalline lattice due to increased amplitudes of the atoms' oscillations around their equilibrium positions. The third contribution is related to atomic displacements due to zero vibrations — a purely quantum-mechanical effect. As the latter contribution is usually small at $T = 0$ K, it is often neglected. The fact that this contribution is difficult to detect experimentally is also of importance. There is, however, an important exception to this rule. It is related to isotope substitution. Inasmuch as, in this case, the chemical substances are identical (this practically is the same substance), the first contribution (atomic size) is constant for substances containing different isotopes. A difference in the lattice constant will, therefore, be fully determined by the differences in thermal expansion and displacements due to zero vibrations. The differences mentioned are indeed great for lithium hydride and its isotopic analogs, lithium deuteride and lithium tritide. This follows mainly from the big change in the mass at isotope substitution and, therefore, from a big change in the reduced mass of the unit cell.

The results of many experimental studies have shown that crystals with light isotopes have a significantly larger lattice parameter and a smaller thermal expansion coefficient [129 – 132] as compared to crystals with heavier isotopes. It has many times been stressed that the effects described are most visible at low temperatures. Let us add that this important conclusion is self-consistent. According to the above discussion, a smaller value of the Debye temperature ensures a greater value of the heat capacity (cf. Ref. [75]) at low temperatures and, through the Grüneisen relation, a greater value of the thermal expansion coefficient.

Using the Einstein free energy function, London [133] arrived at the following expression:

$$\frac{M}{V}\,\frac{\mathrm{d}V}{\mathrm{d}M} = \frac{\gamma\beta}{V}(U - E_0 - TC_V)\,\frac{\mathrm{d}\ln v}{\mathrm{d}\ln M}\,, \qquad (69)$$

where V is the molar volume, M is the atomic mass, γ is the Grüneisen coefficient ($\gamma = \alpha V/\beta C_V$, where α is the volume expansion coefficient), β is the compressibility, C_V is the molar heat capacity, E_0 is the potential energy, v is the phonon frequency, and U is the full energy. For monatomic

solids, we have

$$\frac{\mathrm{d}\ln v}{\mathrm{d}\ln M} = -\frac{1}{2}\,, \tag{70}$$

where $\mathrm{d}v/\mathrm{d}M$ can be expressed through the Debye function with a characteristic Debye temperature θ_D. At high temperatures, one can expand the Debye function in a series in the parameter $(\theta_\mathrm{D}/T)^2$. Then, Eqn (69) takes the form

$$\frac{M}{V}\,\frac{\mathrm{d}V}{\mathrm{d}M} = -\frac{1}{20}\,\alpha T\left(\frac{\theta_\mathrm{D}}{T}\right)\left[1+\frac{11}{420}\left(\frac{\theta_\mathrm{D}}{T}\right)^2+\ldots\right], \tag{71}$$

and at $T = 0$ K we have

$$\frac{M}{V}\,\frac{\mathrm{d}V}{\mathrm{d}M} = -\frac{9}{16}\,\frac{\gamma\beta}{V}\,R\theta_\mathrm{D}\,. \tag{72}$$

In the last equation, R is the gas constant.

For two-atomic cubic crystals with atomic masses M and m (see also Ref. [65]), we have

$$v^2 \propto \left(\frac{1}{M}+\frac{1}{m}\right). \tag{73}$$

Thus,

$$\frac{\mathrm{d}\ln v}{\mathrm{d}\ln M} = -\frac{1}{2}\,\frac{1}{[1+(M/m)]}\,. \tag{74}$$

As a result, we arrive at the following expression:

$$\frac{M}{V}\,\frac{\mathrm{d}V}{\mathrm{d}M} = -\frac{1}{20}\,\alpha T\left(\frac{\theta_\mathrm{D}}{T}\right)^2\frac{1}{1+M/m}\,. \tag{75}$$

As has been pointed out by London [133], to give a more exact description of this dependence one needs more detailed information on the phonon frequency spectrum, because the dependence of v on M is complicated. Add that a comparison between the theory and experiment carried out by London has shown good agreement between them (for more details see Ref. [133]).

Lithium hydride. The dependence of the lithium hydride lattice constant on isotope composition has been the subject of many experimental and theoretical studies [44, 134–138] (see also the reviews [139, 140]). These studies have shown that, as has been already mentioned above, the lighter isotope corresponds to a greater lattice parameter and a smaller value of the thermal expansion coefficient as compared to the heavier isotope. Following the classical work by London [133], a simple empirical dependence of the lattice parameter on the reduced mass of isotopes in the unit cell has been obtained in Ref. [134]:

$$a = A\mu + B\,. \tag{76}$$

Here, A and B are constants depending, however, on temperature (see also Ref. [141]). The experimentally observed [132, 134] (Fig. 7) nonlinear dependence of the lattice parameter in LiH and LiD (LiT) is sufficiently well described by a second-order polynomial [55]

$$\frac{\Delta a}{a} = \frac{\sqrt{\mu_\mathrm{LiD}}-\sqrt{\mu_\mathrm{LiH}}}{\sqrt{\mu_\mathrm{LiH}/\mu_\mathrm{LiD}}}\left[A+B(T-T_0)+C(T-T_0)^2\right], \tag{77}$$

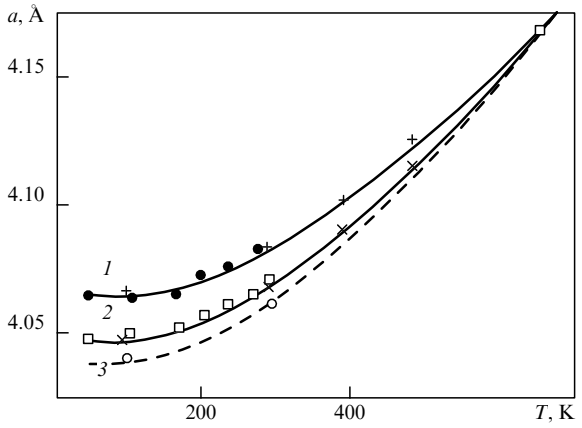

Figure 7. Temperature dependence of the lattice parameter: *1*, LiH; *2*, LiD, and *3*, LiT [55].

where $\Delta a = a_\mathrm{LiH} - a_\mathrm{LiD}$, $1/\mu_\mathrm{LiH} = 1/M_\mathrm{H} + 1/M_\mathrm{Li}$, $T = 25\,^\circ$C, and $\theta_\mathrm{D} = 1080$ K is the Debye temperature of LiH crystals. The constants A, B, and C were determined by the least squares method, and their values are given in Table 6. For comparison we also show the values of these constants found in the same way for the crystals of diamond, silicon, and germanium according to the data of Ref. [23]. According to the calculations of Ref. [55], the lattice parameters of LiH and LiD crystals have the same value at $T = 810$ K, equal to 4.165 Å. This means that the rate of change of $a(T)$ is greater for LiD (the heavier isotope) than for LiH and, in so doing, $\theta_\mathrm{LiD} < \theta_\mathrm{LiH}$. This is a generic statement, because it is valid for covalent crystals as well (for more details see Ref. [70]).

Table 6. Values of coefficients in the polynomial (77) describing a temperature dependence of the lattice parameters at isotope substitution.

Crystal	$A \times 10^3$	$B \times 10^6$	$C \times 10^9$
LiH	55.4	−55.54	−102.8
C	−5.48	3.55	8.2
Si	−1.60	3.94	−6.90
Ge	−0.72	2.27	−6.40

Germanium. Crystals of Ge were the first among semiconducting crystals for which the dependence of the lattice parameter on their isotope composition was studied both theoretically and experimentally [142–144]. In Ref. [144] this dependence has been experimentally studied in high-quality Ge crystal with natural isotope content ($M_\mathrm{av} = 72.59$) and in highly enriched Ge, containing 95.8% ^{74}Ge ($M_\mathrm{av} = 73.93$). To describe the observed dependence, the authors of [143] have used an equation [analogous to (77)] of the form

$$\frac{\Delta a}{a} = -\frac{C}{a^3}\,\frac{\Delta M}{M}\left(\gamma_\mathrm{o}\hbar\omega_0+\frac{3}{4}\,\gamma_\mathrm{a}k_\mathrm{B}\theta_\mathrm{D}\right), \tag{78}$$

where $\gamma_\mathrm{o} = 1.12$ and $\gamma_\mathrm{a} = 0.40$ are the Grüneisen parameters for optical and acoustic photons, respectively; $\theta_\mathrm{D} = 374$ K is the Debye temperature, and $\hbar\omega_0 = 37.3$ meV. With the help of (78), Buschert and coauthors have obtained a decrease in the lattice parameter by 12×10^{-6} and 6×10^{-6} at $T = 0$ and 300 K, respectively. The observed decrease in the lattice parameter in Ge is more than three orders of magnitude less than that observed in LiH crystals. After this paper, two

theoretical papers [23, 144] and one experimental paper [145] appeared. Results agreeing with those already published on the isotope dependence of the lattice parameter in crystals have been obtained in [144, 145]. Note, in passing, that in Ref. [146] the isotope dependence of the lattice parameter of silicon crystals has been studied theoretically.

Diamond. Dependence of the lattice parameter on the isotope composition of diamond crystals has drawn attention in relation to experiments on thermal conductivity (see paragraph 3.2). Banholzer and collaborators [147] have published the values of the lattice parameters in natural diamond and grown ^{13}C, obtained from the X-ray diffraction pattern that were taken from powder and crystalline specimens. Studies of the dependence of the lattice parameter of isotopically mixed crystals were made by Holloway and collaborators [45, 86]. According to Ref. [45], isotope dependence of the lattice parameter of diamond is, analogously to the case of LiH, a linear function of the isotope concentration x and has the form

$$a(x) = 3.56714 - 5.4 \times 10^{-4} x\,. \tag{79}$$

Dependence of the lattice parameter on the isotope concentration in diamond crystals with a different isotope composition has been studied by Yamanaka and collaborators [46]. They have shown that a change in the lattice parameter lies in the interval $(5-9)\times 10^{-5}$ Å and is, once again, three orders of magnitude less than the corresponding variations in LiH crystals. The authors of Ref. [46] described the isotope dependence found in their experiments (Fig. 8) using the following second-order polynomial:

$$a(x) = 3.56712 - 9.0 \times 10^{-4} x + 3.7 \times 10^{-4} x^2\,, \tag{80}$$

where $x = [^{13}C]/[^{12}C + {}^{13}C]$. Equation (80) is not in agreement with the linear dependence of $a(x)$ obtained in Ref. [45]. One of the reasons for this disagreement could be different values of compressibility and Grüneisen parameters for different isotopes (for more details see Ref. [55]). Concluding this section, let us note that by now an isotope dependence of the lattice parameter has also been observed in GaAs and ZnSe crystals [25, 26, 77]. It is necessary to point out the absence of the isotope effect for the lattice parameter in KCN crystals [148].

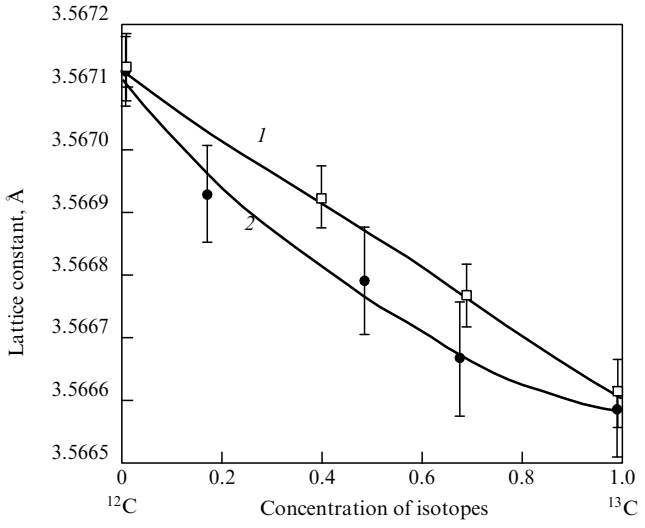

Figure 8. Isotopic dependence of the lattice constant of diamond crystals: *1*, linear dependence obtained in Ref. [45]. Concentration of isotopes was calculated by the formula $x = [^{13}C]/[^{12}C + {}^{13}C]$; *2*, quadratic dependence described by equation (80) obtained in Ref. [46].

4. Vibrational properties

4.1 Dispersion curves and density of phonon states

The main characteristics of a phonon spectrum are the dispersion relation $\omega(q)$ and the frequency distribution function $g(\omega)$ [149]. Both are mainly determined in experiments on the scattering of thermal neutrons, provided it turns out to be possible to separate coherent and incoherent scattering. An important role of neutrons in studying lattice dynamics is related to the fact that the energy of thermal neutrons ($k_B T \sim 10^{-1} - 10^{-2}$ eV) is of the same order as the energy of phonons. At the same time their de Broglie wavelength is comparable with the interatomic distance in crystals. In this respect neutrons have advantages over electromagnetic waves, for which one can only obtain agreement either in energy (IR range), or in wavelength (γ radiation). Special features of the scattering of thermal neutrons by the lattice are determined by the following main factors.

1. Since the neutron wavelength is much larger than the size of the nucleus, the scattering is isotropic and does not depend on the neutron's energy.

2. Scattering of neutrons by the first nucleus is described, with good accuracy, by the Fermi pseudopotential proportional to the δ function:

$$U_l(\mathbf{r}) = \frac{2\pi\hbar^2 b_l}{m_n}\,\delta(\mathbf{r} - \mathbf{R}_l)\,, \tag{81}$$

where m_n is the neutron mass and b_l is the so-called scattering length.

3. The total cross section of scattering on the ensemble of nuclei forming the crystal is determined by summing over the individual nuclei with due account for the phase relations for the scattered waves. If the nuclei oscillate, the neutron scattering can be both elastic and inelastic, i.e., can be accompanied by the creation or annihilation of one or several phonons.

4. The scattering length b_l can strongly differ for isotopes of one and the same element. In addition, for nonzero nuclear spin, b_l depends on the relative orientation of the spins of the neutron and nucleus. It is precisely these factors that lead to the appearance of incoherent scattering, i.e., such scattering, in which the momentum conservation does not hold due to the violation of translational symmetry (for more details see Ref. [150]).

The principle of the measurement of phonon dispersion with the help of one-phonon coherent scattering can be easily understood from energy and momentum conservation

$$E_i - E_s = \frac{\hbar^2}{2m}(\mathbf{k}_i^2 - \mathbf{k}_s^2) = \hbar\omega_j(\mathbf{q})\,, \tag{82}$$

$$\mathbf{Q} = \mathbf{k}_i - \mathbf{k}_s = \mathbf{q} + \mathbf{G}\,, \tag{83}$$

where E_i and E_s are the energies of the incident and scattered neutrons, $\hbar\mathbf{k}$ are their momenta, $\mathbf{G}$ is the reciprocal-lattice vector, $\mathbf{Q}$ is the phonon vector, and j is the index of the phonon spectrum branch. Measuring the neutron velocities before and after interaction, one finds from (82) the frequency

of the phonon that participated in the scattering process. If, in addition, one measures the scattering angle, then, with the help of (83), one can calculate the values of the phonon wave vector **q**, thus completely determining the dispersion relation in one point of the Brillouin zone. In reality the situation is complicated by the presence, at a given **q**, of several frequency values. In other words, for each value of transferred momentum **Q** there exist several groups of neutrons scattered at each branch (for more details see Ref. [149]).

For incoherent scattering there holds only the law of energy conservation (82), so that the energy spectrum of scattering turns out to be continuous in the limits of $E_i \pm \hbar\omega_{max}$. The scattering cross section is proportional to the frequency distribution function $g(\omega)$, but also contains one more frequency-dependent multiplier, which is a function of phonon polarization vectors $\mathbf{e}^s(\mathbf{q})$ [150]. Thus, the function $g(\omega)$ reconstructed from experimental data reflects to a certain degree the model used for determining the polarization vectors.

In the case of lithium hydride crystals, the scattering of neutrons is strongly dependent on the isotope composition. The nonzero spin of the hydrogen nucleus leads to very strong incoherent scattering, so that for lithium hydride one can measure the frequency distribution function but not the dispersion relation. On the contrary, in LiD (with 100% content of D) only coherent scattering takes place. However, already a small percentage of hydrogen in LiD allows one to observe incoherent scattering as well.

Measurements of the scattering of thermal neutrons by LiH (LiD) crystals were carried out in Refs [151, 152]. In the paper by Zemlyanov et al. [151], the incoherent scattering of neutrons was measured. In Figure 9a we show the dispersion curves for lithium deuteride obtained in [152]. According to the estimate of the authors, the accuracy of these data constitutes 3–4%. In spite of the serious efforts undertaken by the authors of [152], it has turned out to be impossible to observe the scattering by longitudinal optical phonons. This has been interpreted as a consequence of the small lifetime of LO phonons (see also Ref. [70] and references therein). To describe experimental results, the authors of Ref. [152] have used a shell model with seven parameters: A^{+-} and B^{+-} are the constants of the short-range potential of the interaction of nearest neighbors; A^{--} and B^{--} are the same constants for the interaction of nearest anions; Z is the effective charge; α and d are the electric and 'mechanical' polarizabilities of the deuterium ion, respectively (cations were considered to be nonpolarizable). All the parameters mentioned were determined from a condition of reaching the best agreement of calculation with experimental results. The values of the parameters obtained in this way are given in Table 4 of Ref. [55].

The solid curves in Fig. 9a correspond to dispersion curves calculated with the above-described values of parameters. It is seen that, as should have been expected (see also Ref. [70]), the maximum deviation is observed in the vicinity of the point L of the Brillouin zone. Using the obtained values of parameters, one can calculate elastic and dielectric characteristics and compare them with experimental data. Add that the ionicity $Z = 0.88$ obtained in the shell model agrees well with the above-presented estimates.

As has already been mentioned, for LiH crystals it is impossible to measure the dispersion curves. Following the authors of Ref. [152] it is, however, reasonable to assume that with good accuracy all parameters of the model remain the same — excluding, of course, the anion masses for LiH and LiD crystals. Dispersion curves calculated within this assumption in Ref. [152] are published in Ref. [55]. The shell model correctly predicts not only the values of the frequencies of TO and LO phonons, but also of other phonons found from absorption spectra of the color centers in LiH crystals [153].

In Figure 9b, frequency distribution functions $g(\omega)$ calculated within the shell model for the crystals of lithium hydride and deuteride (see, for example, Ref. [55]) are shown. We see that the spectral distribution of phonons in LiH and LiD is practically the same in the acoustic vibration range (~ 450 cm^{-1}). At the same time the optical zone in LiH is $\sqrt{2}$ times broader than in LiD. This follows from the fact that in a crystal lattice with significantly different ion masses the main participants of acoustic vibrations are the heavy ions, whereas the light ones mainly participate in the optical vibrations. Besides that, in the $g(\omega)$ distribution of LiH crystals a narrow gap in the interval from 583 to 608 cm^{-1} is present, which is absent for LiD. It is appropriate to add that in LiH the frequency of the transverse optical phonon corresponds to the edge of the gap, so that the density of states corresponding to this frequency is very small.

Very accurate measurements of diamond dispersion curves have been carried out in Ref. [154], those of silicon (Fig. 10a) in Ref. [155], and germanium in Ref. [156]. Numerous theoretical computations of phonon dispersion curves in crystals, Refs [58, 154, 157], show good agreement with experiment, except for the diamond crystal.

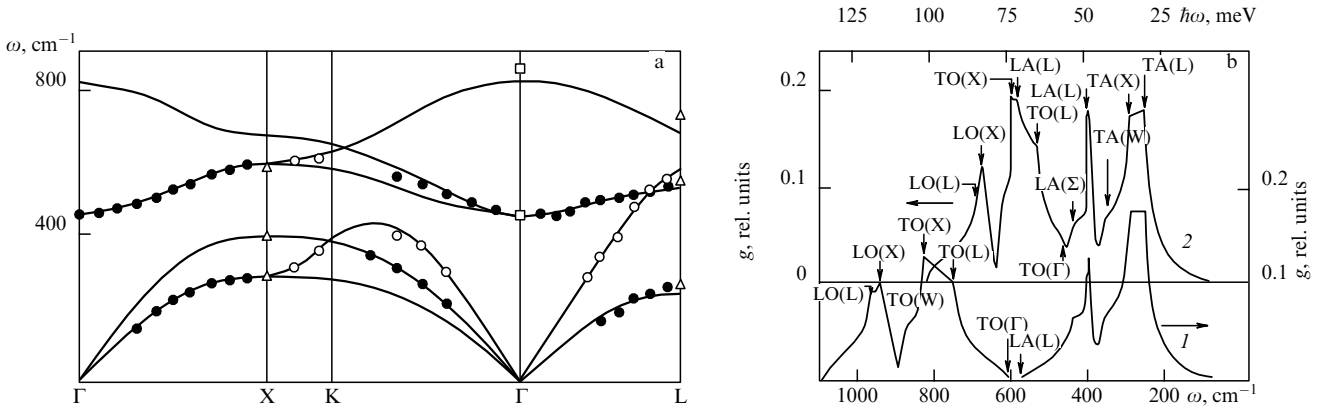

Figure 9. (a) Dispersion curves of phonons in the crystal of ^{7}LiD [55]; and (b) phonon frequency distribution function $g(\omega)$ in LiH (*1*) and LiD (*2*) crystals [141].

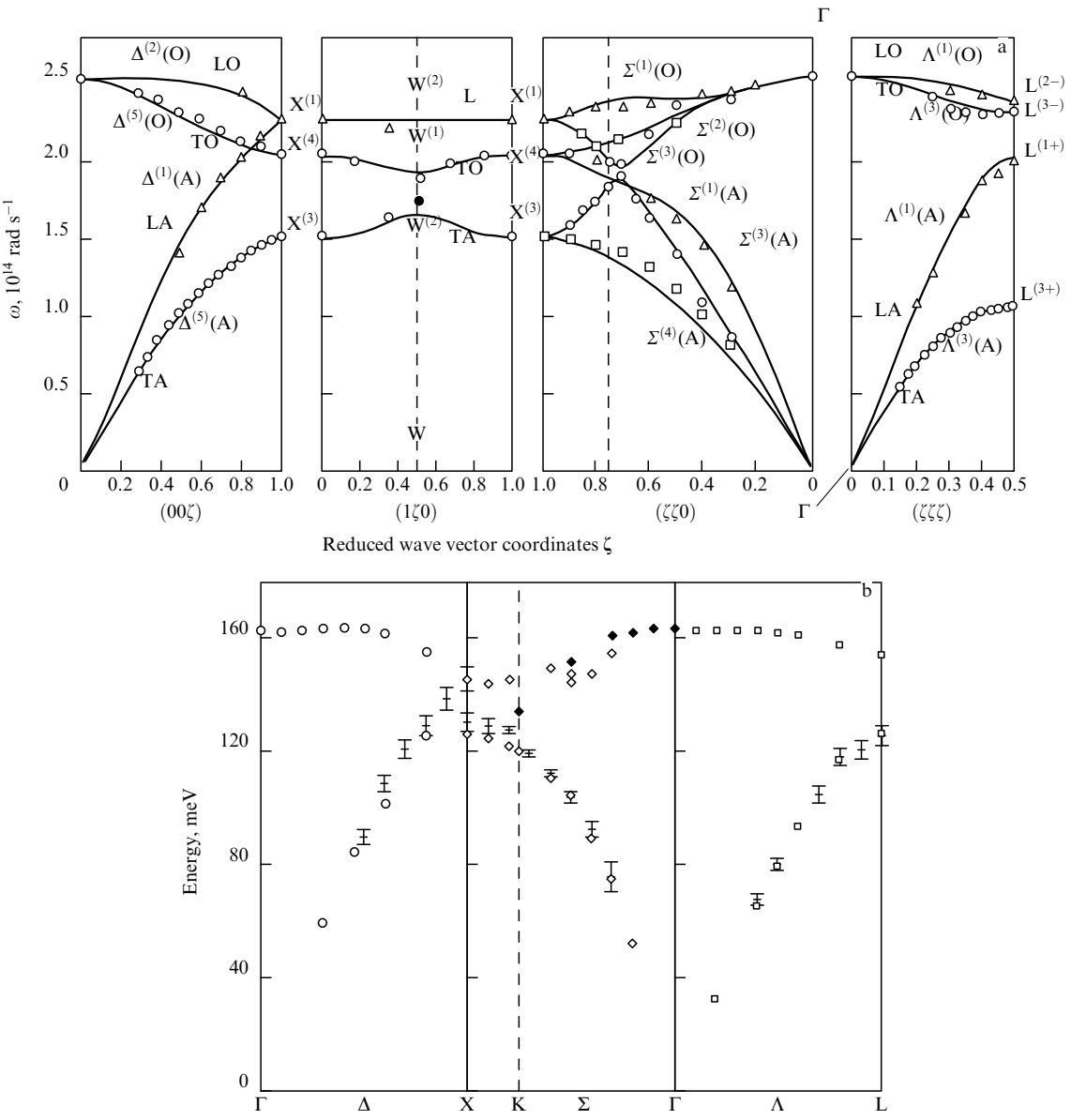

Figure 10. (a) Phonon dispersion curves in silicon at room temperature [155] and (b) a comparison of the dispersion curves of diamond with the theoretically calculated ones [159].

The unusual properties of diamond, e.g., the small value of the lattice parameter, the unusually large value of the volume compression modulus, etc., are well known [67, 78, 120, 141]. Besides this, diamond is characterized by the presence of a maximum in the dispersion curve that is located not at the Γ point of the Brillouin zone. In this respect, much interest in the lattice dynamics of diamond has always been drawn by the presence of a narrow peak in the two-phonon density of phonon states (Fig. 11a), located 2 cm^{-1} higher than the doubled value of the energy of LO phonons. This picture is sharply different from the two-phonon density in Ge and Si. Such a singularity in the two-phonon density of phonon states has traditionally been related to the bending of the dispersion curve along the Δ direction (for more details see Ref. [70]). Very recently, such a behavior of the dispersion relation was obtained in Ref. [160]. However, in the cited work a shift of the peak, equal to 25 cm^{-1} (~3 meV), has been found to take place above the edge of the phonon spectrum, i.e., an order of magnitude larger than the experimentally observed one. Recently, the character of the diamond dispersion curves was again studied by neutron scattering [161] and inelastic X-ray scattering [159]. The results of the latter study are presented in Fig. 10b. There, we also show, for comparison, theoretical and experimental results. We see that good agreement between theory and experiment takes place. Thus, these studies close the discussion on the nature of the high-energy peak observed in the density of the two-phonon states in diamond (for more details see Ref. [141]).

The two-phonon density of states calculated by the method of the plane-wave pseudopotential in the local density-functional approximation (for more details see Ref. [58]) for diamond [160] and silicon [162] crystals is shown in Fig. 11. As can be seen from Fig. 11a, in accordance with experiment (on Raman light scattering), in the domain above the edge of 2LO phonons a sharp peak, which is not, however, observed in the DOS spectra of Si crystals, is clearly reproduced.

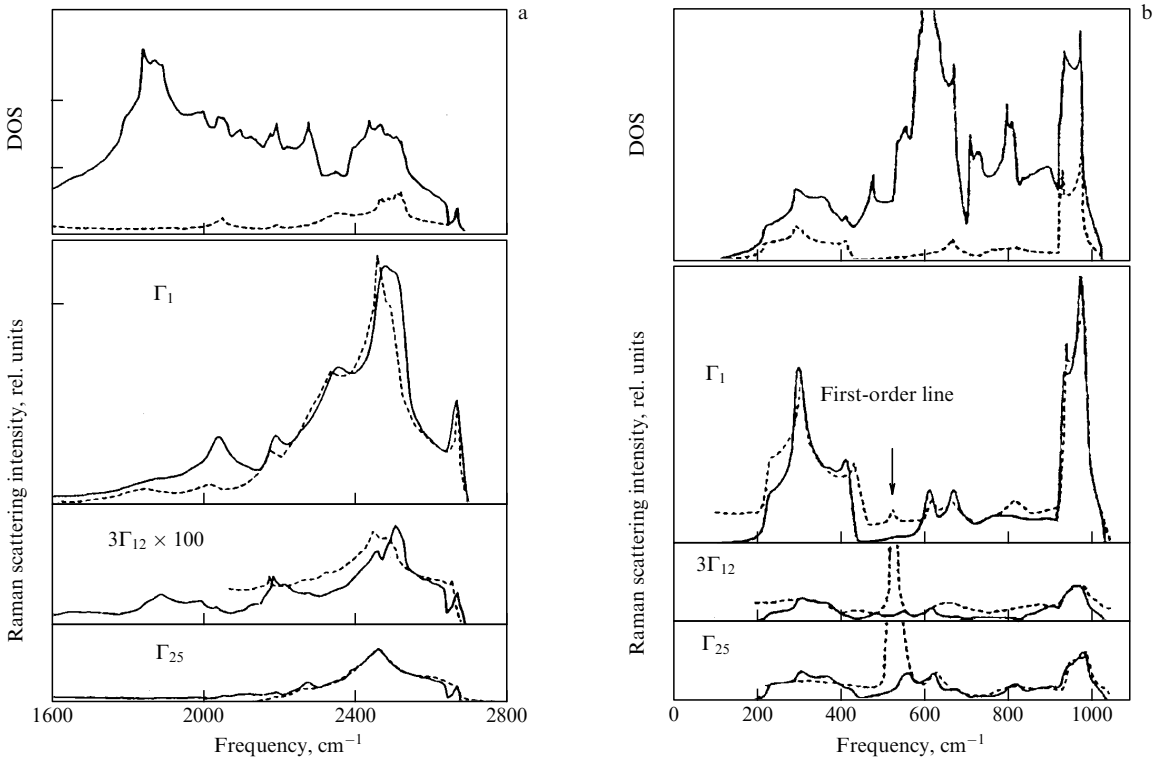

Figure 11. Theoretically computed density of two-photon states in (a) diamond and (b) silicon [160]. The solid line corresponds to the DOS (density of states), the dashed one to the overtone.

4.2 Raman scattering spectra of isotopically mixed single crystals

4.2.1 Small concentrations: local, resonance, and gap vibrations. Studies of vibrational properties of crystals containing impurities (defects of various origin) are sufficiently well described and documented in a number of excellent reviews [33–43]. Traditionally these results are classified as referring to two domains, the domain with a low ($C \leqslant 10\%$) concentration of defects (impurities) and the domain of high ($C \geqslant 10\%$) concentration. The latter, the so-called mixed crystals, will be described in the next section. Here, we analyze the results in the low-concentration domain, i.e., when the interaction between defects (impurities) can be, in the first approximation, neglected [33, 34].

The simplest defects in a crystal lattice that break its translational symmetry are the isotopes of the elements that form the crystal. In the majority of cases, the influence of isotopes on vibrational spectrum is small and is not taken into account in calculations of dispersion curves. The case of the LiH – LiD system is different. A significant change in mass taking place after substitution of D for H displaces the whole zone of optical vibrations by ~ 250 cm^{-1}. It is thus clear that small concentrations of isotopes can also generate substantial effects [141], especially in phenomena related to the motion of the defects themselves [32, 163]. In the case of small concentrations, the main effects consist of the appearance of various processes induced by the defects. For example, an IR absorption of the ideal lattice includes, in harmonic approximation, one delta-shaped peak at the frequency $\omega_{\mathrm{TO}}(\Gamma)$, whereas after introducing defects the selection rule related to the wave vector is lifted, resulting in the appearance of additional absorption in the whole range of frequencies (with intensity proportional to the concentration of defects). For vanishingly small concentrations, one has an adequate theory developed by Lifshitz [33]. In the case of isotope defects this theory does not contain free parameters (see also Ref. [34]). The approach by Lifshitz is based on the technique of Green's functions. Using this method is particularly convenient since it allows one to write a solution of equations describing vibrations in the presence of point defects of various types (for more details see Ref. [164]). The change in the mass of the atom causes the appearance of three types of features in the phonon spectrum [164, 165]: local, gap, and quasi-local (resonance) vibrations. Vibrations of the first type have frequencies located above the maximum frequency of the phonon spectrum and arise in the case of a sufficiently small decrease in the mass of an atom (ion). The frequencies of vibrations of the second type are located in the gap between the optical and acoustic zones. These vibrations can exist both for decreasing and increasing mass. Resonance vibrations arise if the mass of a defect is much larger than that of the replaced ion. They are characterized by sharp maxima in the frequency distribution function in the range $\omega \ll \omega_{\max}$. Frequencies of vibrations of all these types are determined by the following equation [33]:

$$1 = \lambda_s \omega^2 \operatorname{Re} G_0^s(\omega)\,. \tag{84}$$

Here, $\lambda_s = 1 - M_s'/M_s$ (M_s' is the mass of the defect in the sth sublattice) and

$$G_0^s(\omega) = \frac{1}{3N}\sum_{\mathbf{q}j} \frac{\left|\mathbf{e}_s(\mathbf{q}j)\right|^2}{\omega^2 - \omega_{\mathbf{q}j}^2 + \mathrm{i}0} = \frac{1}{3N}\sum_{\mathbf{q}j} \frac{\left|\mathbf{e}_s(\mathbf{q}j)\right|^2}{[\omega^2 - \omega_{\mathbf{q}j}^2]_P} + \mathrm{i}\pi\,\frac{1}{3N}\sum_{\mathbf{q}j}\left|\mathbf{e}_s(\mathbf{q}j)\right|^2 \delta(\omega^2 - \omega_{\mathbf{q}j}^2)\,. \tag{85}$$

In this formula, P denotes the principal value.

In lithium deuteride the condition of the appearance of local vibration after replacing a D ion by an H ion takes the form $M_s'/M_s = 0.66$ [55] (for phonon spectrum in the shell model). Thus, placement of H ions into the lattice of a LiD crystal should lead to the appearance of a local vibration.

In Figure 12a the spectrum of second-order Raman scattering (RS) of light in pure LiD crystal at room temperature [55] is shown. First of all, it is necessary to note the good agreement of this spectrum and those measured earlier [166, 167]. In spite of the fact that, according to the nomogram of the exciton states [168], the crystal studied should be considered to be pure, its RS contains a clear high-frequency peak around 1850 cm^{-1}. The observed peak does not have an analogue in RS spectra of pure LiH and has already been observed earlier in the second-order RS spectra [169] and has been interpreted, starting from Ref. [169], as a local vibration of the hydrogen ion in LiD crystals. The calculated value of ω_{loc} lies in the interval 917–995 cm^{-1}. We see that the peak at $\omega_{loc} = 1850$ cm^{-1} observed in RS agrees well with the doubled value $\omega = 917$ cm^{-1} calculated in the most consistent way. Although the actual concentration of H in the LiD crystals studied is very small (according to Ref. [168], the location of the maximum of the $n = 1S$ line in reflection and luminescent spectra corresponds to the pure LiD crystal), it is, as seen from Fig. 12a, however, sufficient for observing a local mode in the second-order RS spectra.

Calculation of the concentration of hydrogen ions (estimates of concentration in Ref. [168] have been based on the location of the ground-state level of the exciton in reflection spectra) leads [55] to growing intensity of the peak of the local mode and its small high-frequency shift. The described behavior holds for hydrogen ion concentrations $C \leqslant 10\%$. It is necessary to stress that a systematic study of the concentration dependence of the shape of the local mode peak allows us to obtain a detailed understanding of the percolation threshold separating the local phonon states from the extended ones (see also Refs [70, 141]). Based on the RS spectra studied in [55, 141], in Fig. 12b the dependence of the local vibration frequency on hydrogen ion concentration was constructed. In Figure 12b we also show a theoretical calculation of the $\omega_{loc} \sim f(x)$ dependence from Refs [169–171]. In Ref. [170] a concentration dependence of the frequency and intensity of the local mode in LiH_xD_{1-x} has been calculated with the help of a temperature Green's function. For the calculation, a model phonon spectrum containing two Gaussian bands and limited by the frequency interval $\omega_{TO} < \omega < \omega_{LO}$ (as became clear after the work by Verble et al. [152], this approximation is not quite satisfactory) was used. Using the real phonon spectrum of LiD crystal measured in Ref. [152], the authors of Ref. [171] have repeated, in the framework of the model of deformed dipoles, the calculation of the concentration dependence of frequency and intensity of the local mode. As has already been mentioned above, the calculated values for ω_{loc} obtained in Refs [169, 170] are close to each other, but are somewhat higher than the values obtained in the improved calculation of Ref. [171], where the result was $\omega_{loc} = 917$ cm^{-1}. More serious disagreements in the $\omega_{loc} \sim f(x)$ dependences were found in Refs [170, 171]; namely, according to the results of Ref. [171], the value of ω_{loc} grows with x, whereas it decreases according to Ref. [170]. In spite of this disagreement, it is necessary to stress the good agreement in the variation of the intensity of the local-mode band as a function of concentration found in the above-cited papers (see also Ref. [55]). The experimentally observed [55] $\omega_{loc} \sim f(x)$ dependence is practically parallel to the theoretical one calculated in Ref. [169], but is shifted to lower values (Fig. 12b). On the other hand, it agrees very well with the newly calculated value of ω_{loc} at $x = 0$ from Ref. [171]. From this, one can conclude that the model of deformed dipoles describes the behavior of the local mode related to vibrations of hydrogen ions in the lithium deuteride crystals sufficiently well. After introduction of deuterium ions into LiH crystal there appears a gap excitation. Its sufficiently detailed analysis has been performed in a number of publications (see, e.g., Refs [55, 141, 172]).

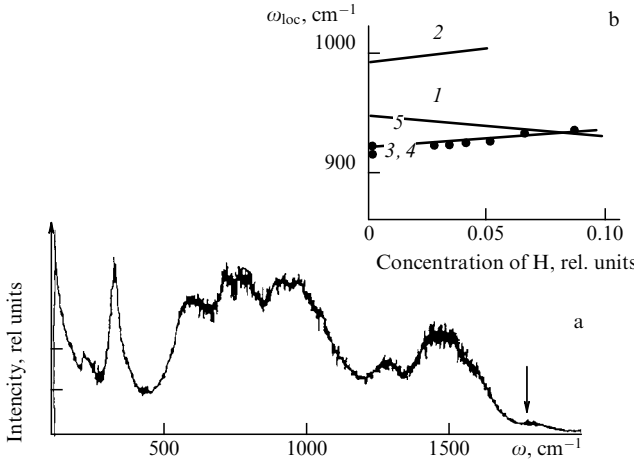

Figure 12 (a) Raman spectrum of light scattering in LiD crystals at room temperature [55] and (b) concentration dependence of the local vibration frequency in LiD crystals at room temperature [141].

4.2.2 Large concentrations: isotopically mixed crystals. If an impurity content in the crystal rises to such a limit that interaction between the impurity atoms (ions) becomes essential, it is customary to describe these systems as mixed crystals with different degrees of disorder. One distinguishes two types of disorder: disordered alloys (isotope mixtures); and mixed crystals and glassy systems with a more pronounced spatial disorder than the configurational one. One can consider, as a first theoretical model of the dynamics of mixed crystals, a linear chain model that develops the virtual-crystal model by Nordheim [173]. In spite of its simplicity, the model describes the general features of the lattice dynamics of mixed alkali-halide crystals sufficiently well. In this model two independent force constants f and f' are introduced. As a rule, they are determined from the formula $f = \omega^2 m M/2(m + M)$, where ω are the observed frequencies of LO phonons of pure substances, and m and M are the masses of crystal-forming particles. Concentration dependence of the force constant is described by the relation $F = f'x - (f' - f)x$, assuming that the growth (decay) of $f(f')$ as a function of concentration is linear (see, e.g., Ref. [37]). Allowance for the more complex dependence of the force constant, as well as a description of the cluster and isoshift models in lattice dynamics using the coherent potential approximation [37, 42, 174] or T-matrix averaging (see, e.g., Refs [36, 41]), are described in the exhaustive reviews of Refs [37–39, 42].

First-order scattering spectra. Semiconducting crystals (C, Si, Ge, α-Sn) with a diamond-type structure present ideal

objects for studying the isotope effect by the Raman light-scattering method. At present this is facilitated by the availability of high-quality crystals grown from isotopically enriched materials. In this section, the modern understanding of first-order Raman light scattering spectra in isotopically mixed elementary and compound (CuCl, GaN, GaAs) semiconductors having a zinc blende structure is described. Isotope effect in light scattering spectra in Ge crystals was first investigated in the paper by Agekyan et al. [21]. A more detailed study of Raman light scattering spectra in the isotopically mixed Ge crystals has been performed by Cardona and coworkers [175 – 177].

It is known that materials having a diamond structure are characterized by the triply degenerate phonon states in the Γ point of the Brillouin zone ($\mathbf{k} = 0$). These phonons are active in the Raman scattering spectra, but not in the IR absorption ones [178]. Figure 13a demonstrates the dependence of the shape and position of the first-order line of optical phonons in germanium crystal on the isotope composition at liquid-nitrogen temperatures [175]. The coordinate of the center of the scattering line is proportional to the square root of the reduced mass of the unit cell, i.e., $\sqrt{M}$. It is precisely this dependence that is expected in the harmonic approximation. An additional frequency shift of the line is observed for the natural and enriched germanium specimens and is equal, as shown in Refs [176, 179], to 0.34 ± 0.04 and 1.06 ± 0.04 cm^{-1}, respectively (see, e.g., Fig. 7 in Ch. 4 of Ref. [70]).

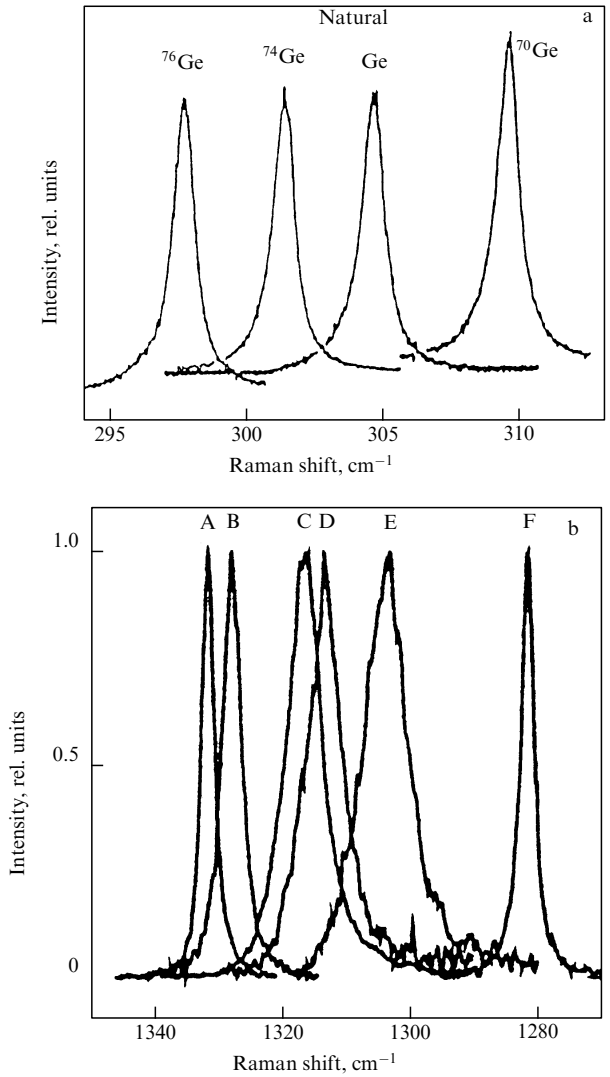

Figure 13. (a) First-order Raman scattering spectra in Ge with different isotope contents [175] and (b) first-order Raman scattering spectra in isotopically mixed diamond crystals $^{12}C_x\,^{13}C_{1-x}$. The peaks A, B, C, D, E, and F correspond to $x = 0.989$; 0.90; 0.60; 0.50; 0.30, and 0.001 [180].

First-order Raman light-scattering spectrum in diamond crystals also includes one line with the maximum at $\omega_{LTO}(\Gamma) = 1332.5$ cm^{-1}. In Fig. 13b, the first order scattering spectrum in diamond crystals with different isotope concentrations is shown [180]. As shown below, the maximum and the width of the first-order scattering line in isotopically-mixed diamond crystals are nonlinearly dependent on the concentration of isotopes x. The maximum shift of this line is 52.3 cm^{-1}, corresponding to the two limiting values of $x = 0$ and $x = 1$. Analogous structures of first-order light scattering spectra and their dependence on isotope composition has by now been observed many times, not only in elementary Si [181] and α-Sn [177], but also in compound CuCl [182] and GaN [176] semiconductors (for more details see Ref. [141]). Already this short list of data shows a large dependence of the structure of first-order light-scattering spectra in diamond as compared to other crystals (Si, Ge). This is the subject of a detailed discussion in Section 3.3.

Second-order scattering spectra. Second-order Raman scattering spectra in natural and isotopically mixed diamond crystals have been studied by Chrenko [19] and Hass et al. [183]. Second-order Raman scattering spectra in a number of synthetic diamond crystals with different isotope compositions shown in Fig. 14 are measured with resolution (~ 4 cm^{-1}) worse than for first-order scattering spectra. The authors of the cited work explain this fact by the weak signal in the measurement of second-order Raman scattering spectra. It is appropriate to note that the results obtained in Ref. [183] for natural diamond ($C_{^{13}C} = 1.1\%$), agree well with the preceding comprehensive studies of Raman light-scattering spectra in natural diamond crystals [184]. As is clearly seen from Fig. 14, the structure of second-order light scattering 'follows' the concentration of the ^{13}C isotope. It is necessary to add that in the paper by Chrenko [19] one observes a distinct small narrow peak above the high-frequency edge of LO phonons and at the concentration of ^{13}C $x = 68$ at. %. Note in passing that second-order spectra in isotopically mixed diamond crystals were measured in the work by Chrenko [19] with a better resolution than the spectra shown in Fig. 14.

Second-order Raman [185] and IR absorption [186] light-scattering spectra in crystals of natural and isotopically enriched ^{70}Ge measured at 100 K are shown in Fig. 15, which distinctly demonstrates the influence of the isotope composition of Ge on the DOS spectrum. We see that the dominant effect of the isotope shift and broadening is observed in a high-frequency, i.e., optical, part of the DOS spectrum. The clearest illustration of this is given in Fig. 16, where the maximum broadening of the spectra is observed for 2TO (W) and 2TO (L) phonons in natural Ge, as compared to the isotopically enriched ^{70}Ge.

A comprehensive interpretation of the whole structure of second-order Raman light-scattering spectra in pure LiH (LiD) crystals is given in Refs [167, 76, 187, 188]. Leaving this question, let us now analyze the behavior of the highest frequency peak after the substitution of hydrogen for deuterium (see also Ref. [141]).

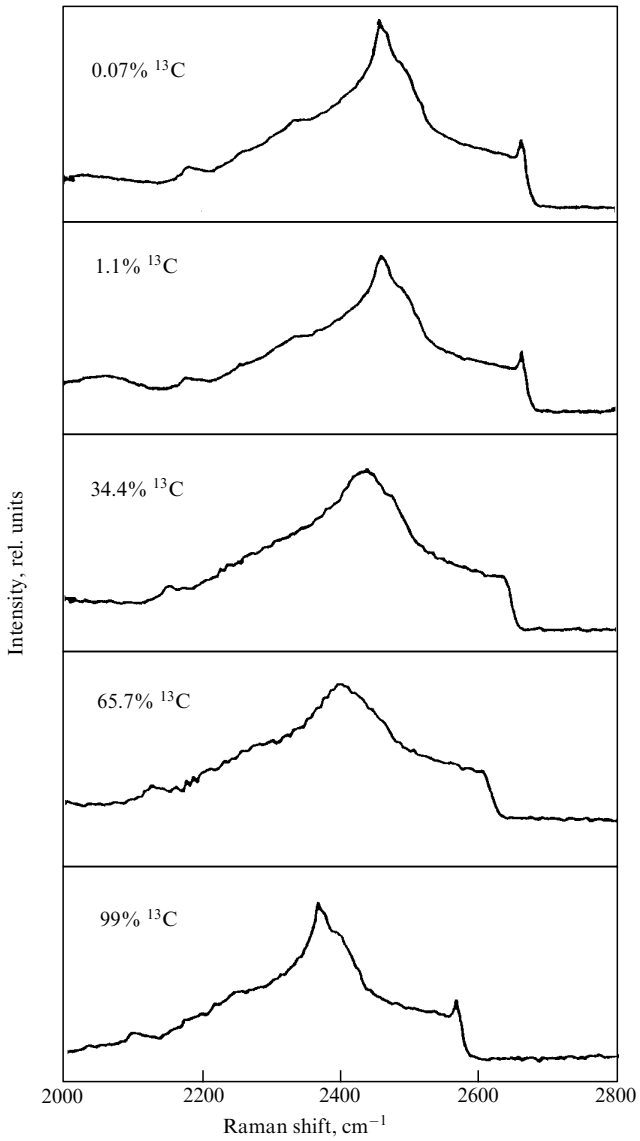

Figure 14. Second-order Raman scattering spectra in synthetic diamond with different isotope concentrations at room temperature [183].

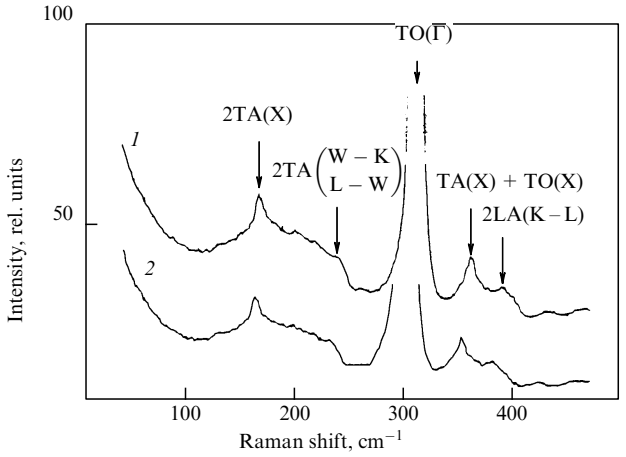

Figure 15. Optical part of the second-order Raman light scattering spectra in isotopically enriched germanium ^{70}Ge (*1*) and natural Ge (*2*) [185].

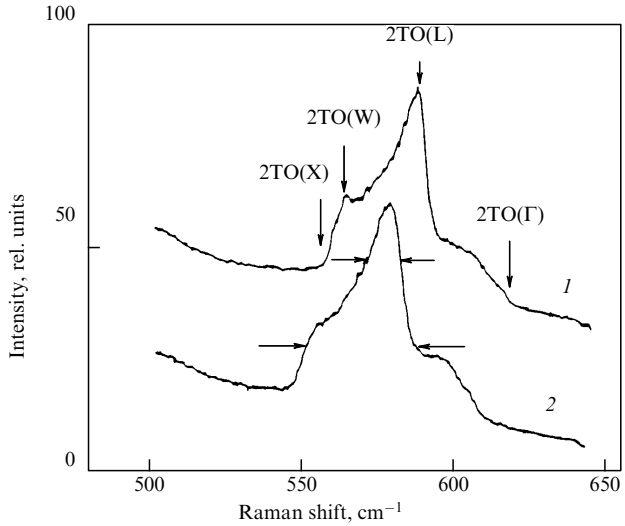

Figure 16. Comparison of calculated optical density of states (DOS) in (*1*) isotopically enriched germanium ^{70}Ge and (*2*) natural Ge [185].

Absorption behavior of an IR-active phonon in mixed crystals with a change in the concentrations of the components can be classified into two main types: one- and two-mode (see, e.g., the review [42]). Single-mode behavior means that one always has a band in the spectrum with a maximum gradually drifting from one endpoint to another. Two-mode behavior is defined by the presence, in the spectrum, of two bands characteristic of each component of the mixed crystal. Changes in the concentration of the components lead not only to changes in the frequencies of their maxima, but mainly to a redistribution of their intensities. In principle, one and the same system can show different types of behavior at opposite ends [38]. The described classification is qualitative and is rarely realized in its pure form (see also Ref. [41]). The most important necessary condition for the two-mode behavior of phonons (as well as of electrons [189]) is considered to be the appearance of the localized vibration in the localized-defect limit. In the review of Ref. [42] a simple qualitative criterion for determining the type of the IR absorption behavior in crystals with an NaCl structure type has been proposed (see also Ref. [189]). Since the square of the TO(Γ) phonon frequency is proportional to the reduced mass of the unit cell M, the shift caused by the defect is equal to

$$\Delta = \omega_{\mathrm{TO}}^2\left(1 - \frac{\overline{M}}{\overline{M}'}\right). \tag{86}$$

This quantity is compared in Ref. [42] with the width of the optical band of phonons which, neglecting acoustical branches and using the parabolic dispersion approximation, is written as

$$W = \omega_{\mathrm{TO}}^2\left(\frac{\varepsilon_0 - \varepsilon_\infty}{\varepsilon_0 + \varepsilon_\infty}\right). \tag{87}$$

A local or gap vibration appears, provided the condition $|\Delta| > (1/2)W$ is fulfilled. As mentioned, however, in Ref. [42], in order for the two peaks to exist up to concentrations on the order of ~ 0.5, a stronger condition $|\Delta| > W$ has to be met. Substituting the numerical values from Tables 1 and 2 into formulas (86) and (87) shows that for LiH (LiD) there holds

(since $\Delta = 0.44\omega_{TO}^2$ and $W = 0.58\omega_{TO}^2$) the following relation:

$$|\Delta| > \frac{1}{2} W. \tag{88}$$

Thereby it follows that at small concentrations the local vibration should be observed. This conclusion is in perfect agreement with the earlier described (Fig. 12a) experimental data. As to the second theoretical relation $\Delta > W$, one can see from the above discussion that for LiH (LiD) crystals the opposite relation, i.e., $W > \Delta$, is observed [55].

Following the results of Ref. [49], in Fig. 17 we show the second-order RS spectra in mixed LiH_xD_{1-x} crystals at room temperature. In addition to what has been said on RS spectra at high concentrations (see Ref. [49]), we note that as the concentration grows further ($x > 0.15$) one observes in the spectra a decreasing intensity in the maximum of 2LO(Γ) phonons in LiD crystal with a simultaneous growth in intensity of the highest frequency peak in mixed LiH_xD_{1-x} crystals. The nature of the latter is in the renormalization of LO(Γ) vibrations in mixed crystal [190]. Comparison of the structure of RS spectra (curves *1* and *2* in Fig. 17) allows us, therefore, to conclude that in the concentration range of $0.1 < x < 0.45$ the RS spectra simultaneously contain peaks of the LO(Γ) phonon of pure LiD and the LO(Γ) phonon of the mixed LiH_xD_{1-x} crystal. For further concentration growth ($x > 0.45$), one could mention two effects in the RS spectra of mixed crystals. The first is related to an essential reconstruction of the acoustooptical part of the spectrum. This straightforwardly follows from a comparison of the structure of curves *1–3* in Fig. 17. The second effect originates from a further shift of the highest frequency peak toward still higher frequencies, related to the excitation of LO(Γ) phonons. The limit of this shift is the spectral location of the highest frequency peak in LiH. This is especially clearly seen when comparing curves *2* and *4* in Fig. 17. Finishing our description of the RS spectra, it is necessary to note that a resonance intensity growth of the highest frequency peak is observed at $x > 0.15$ in all the mixed crystals (for more details see Ref. [19]).

Using the results described and the data obtained for other crystals [49], in Fig. 18b we plot the dependence of the frequency of the highest frequency structure in the RS spectra of pure and mixed crystals on the concentration of isotopes (curve *1*). In the same plot we also show, for comparison, the dependence (curve *2*) of the frequency of the TO(Γ) phonon band maximum determined from the IR absorption spectrum in thin LiH_xD_{1-x} films [192]. A nonlinear dependence of both curves is clearly seen. Curve *2* has already been discussed when analyzing the concentration dependence of the frequency and intensity of the local mode (for more details see Ref. [141]). Here, we add that, up to now, nobody has been able to give a self-consistent description of the concentration dependence in a broad interval. We stress once again that in the domain of small concentrations the agreement between theory and experiment is sufficiently good. This cannot be said about large concentrations. As seen from the results in Fig. 18b, in the concentration range of $x < 0.45$ one observes a two-mode character of LO(Γ) phonons. This is in direct contradiction with the predictions of the CPA model [42,

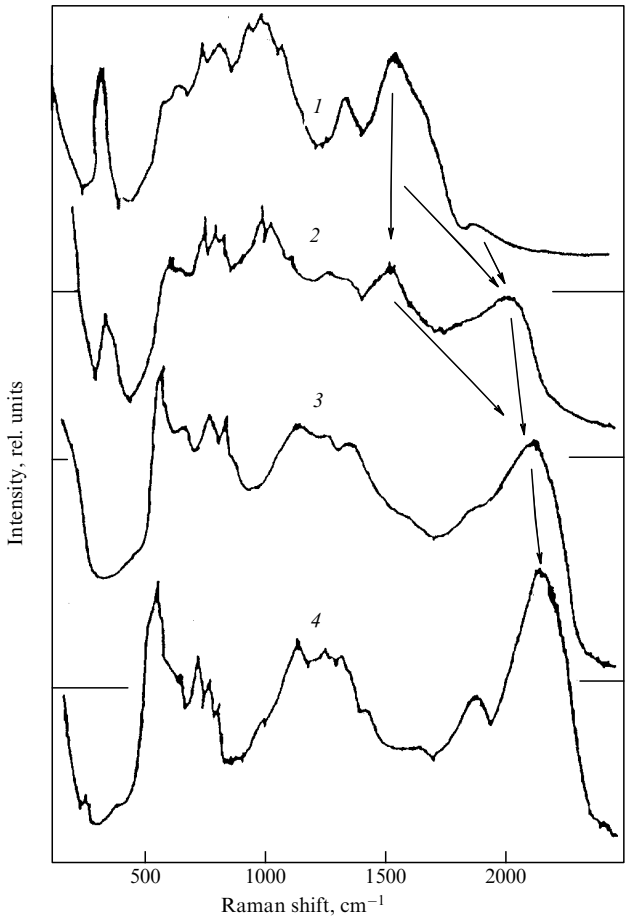

Figure 17. Second-order Raman scattering spectra in the isotopically mixed crystals LiH_xD_{1-x} at room temperature: *1*, $x = 0$; *2*, 0.42; *3*, 0.76; and *4*, 1. The arrows point out a shift of LO(Γ) phonons in the mixed LiH_xD_{1-x} crystals.

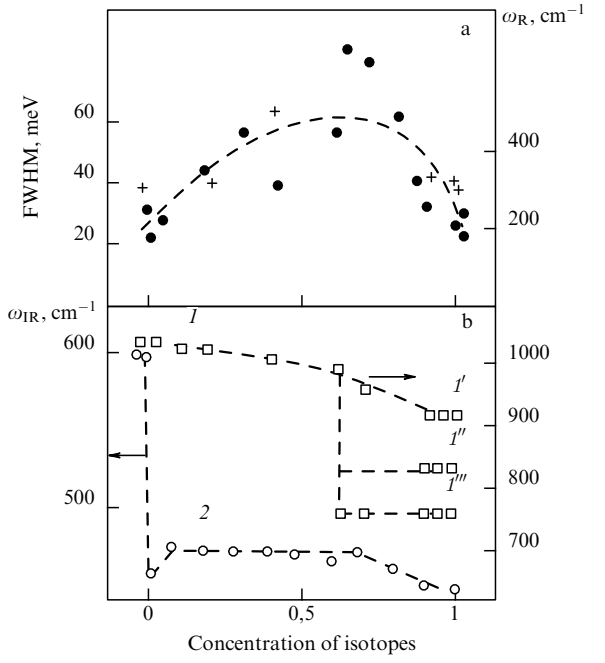

Figure 18. Dependence of (a) the half-width and (b) the frequency of optical phonons in the RS spectra on the concentration of isotopes in isotopically mixed crystals of LiH_xD_{1-x}: (•) the result of Ref. [55]; (+) the results of Ref. [192] on IR absorption of the TO(Γ) phonon in thin LiH_xD_{1-x} films.

194], in which for concentrations $x \sim 0.5$ the width of the band of optical vibrations (W) should be smaller than the shift (Δ) of the frequency of the transverse optical phonon, i.e., $\Delta > W$. At the same time, calculations using formulas (86) and (87) produce, for LiH(LiD) crystals, an inverse relation, i.e., $\Delta > W$ [55]. According to Ref. [49], the observed disagreement between the experimental results and theoretical predictions of the CPA model is primarily related to the strong phonon scattering potential due to a large variation of masses when substituting deuterium for hydrogen. This is also supported by the observation of the local mode in these systems (see Fig. 12). The experimental results presented in this section provide, therefore, evidence of, first, strong scattering potential (most importantly, for optical phonons) and, second, of the insufficiency of the CPA model for a consistent description of these results (see also Ref. [24]).

4.3 Disorder effects in Raman light-scattering spectra of isotopically mixed crystals.

Effects related to isotopic disorder have by now been observed in the phonon states of practically all the isotopically mixed semiconducting crystals, as well as in the well-studied model system LiH – D (see, e.g., Refs [7, 41]). As clearly shown above, a weak scattering of phonons due to isotopic disorder shows itself in the shift and broadening of lines in the RS phonon spectra. On the whole, the data on the isotope shift of the maximum of first-order scattering line in diamond can, in the first approximation, be described in the framework of the virtual-crystal approximation [42]. However, the virtual-crystal model does not include any proper broadening induced, for example, by isotopic disorder in the crystal lattice. To take this into account, in the studies of light scattering in germanium and silicon in Refs [195 – 197], the coherent-potential approximation has been used. As is well known [42, 170], the main idea of the coherent-potential method is in the introduction of an auxiliary medium with a regular, i.e., spatially periodic, potential. By definition, in the model this potential is complex. Therefore, the self-energy of this medium is also complex. The real part of the self-energy describes the frequency shift, and the imaginary part describes the broadening of lines in the spectra of phonon states of isotopically mixed crystals. The formalism of the coherent-potential model is very simple, convenient for performing calculations, and does not include fitting parameters, because of using of the density of phonon states from the virtual-crystal model (VCA) [181, 183]:

$$g_{\mathrm{VCA}}(\omega) = (6N)^{-1} \sum_{\mathbf{q}j} \delta\left(\omega - \omega_{\mathbf{q}j}\right), \qquad (89)$$

where N is the number of cells in the normalized volume, $\mathbf{q}$ is the wave vector of the phonon with a frequency $\omega_{\mathbf{q}j}$, and j is the phonon branch. In the one-phonon scattering case the density of states in the coherent-potential approximation is described by the following expression (see also Ref. [195]):

$$g(\omega) = -\frac{2}{\pi\omega} \int_0^\infty g_{\mathrm{VCA}}(\eta)\, \mathrm{d}\eta\, \mathrm{Im}\left[\frac{\eta^2}{\omega^2\left[1 - \tilde{\varepsilon}(\omega) - \eta^2\right]}\right]. \qquad (90)$$

As shown in Ref. [183], in the case of a weak potential of isotopic scattering of phonons, their self-energy $\varepsilon(\omega)$ does not depend on $\mathbf{q}$. This is precisely the situation observed for C and Ge. Indeed, if we express the mass fluctuation $\Delta M/\overline{M}$ ($\overline{M}$ is the mean mass of all isotopes) in the form of the variation of the phonon band width $\Delta\omega_0 = 12\ \mathrm{cm}^{-1}$ at $\mathbf{q} = 0$ and compare it with the width of the band of optical phonons in Ge equal to $\sim 100\ \mathrm{cm}^{-1}$, we will see that the variation is very small. Under these conditions the localization of optical phonons in Ge is, naturally, absent, and, as observed in the experiment, they stay delocalized. Moreover, direct measurements of the phonon lifetime in Ge show that, in the case of anharmonic decay, it is two orders of magnitude shorter than the lifetime that is due to the additional scattering by isotopes, i.e., $\tau_{\mathrm{anharm}} = \tau_{\mathrm{disord}} \times 10^{-2}$ [175]. Therefore, the contribution of anharmonicity to the half-width of the first-order light scattering line in Ge is two orders of magnitude greater than that caused by the isotopic disorder in crystal lattice.

In Fig. 19a, the $\omega_{\mathrm{LTO}} \sim f(x)$ and $\Delta\omega_{\mathrm{LTO}} \sim f(x)$ dependences in first-order Raman scattering (RS) spectra in diamond found in the virtual-crystal model (VCA) and the coherent-potential approximation (CPA) [183, 198] are comparable. Note, first of all, the good agreement of the results shown in Fig. 19b with the data by Chrenko [19] and Hanzawa et al. [180]. Both sets of data in Fig. 19b demonstrate a nonlinear (with respect to the virtual-crystal model) dependence of both functions on the concentration of isotopes, which is perfectly described in the coherent-potential approximation. Hass et al. [183] have concluded that the observed nonlinear dependence is a direct consequence of an additional phonon scattering due to isotopic disorder in the crystal lattice. Such concentration-related nonlinearity has been observed in many other parameters and properties of alloys (for example, in the energy of interband transitions in semiconducting alloys [199] and isotopically mixed crystals [200]. In diamond, the deviation from linearity for middle isotope concentrations constitutes

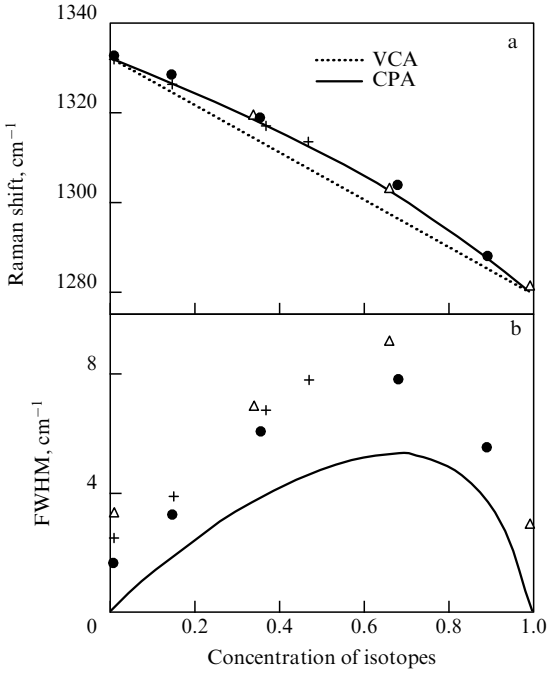

Figure 19. Dependence on the concentration of isotopes of the frequency of the maximum of (a) the LTO phonon scattering line in first-order RS spectra in crystals of diamond and (b) its half-width [198]. The dotted line corresponds to the virtual-crystal approximation; the solid line, to the coherent-potential approximation. Experimental data: (Δ) corresponds to the results of Ref. [183], ($\bullet$) to those of Ref. [19], and ($+$) to the results of Ref. [198].

$\sim 5\ \mathrm{cm}^{-1}$. This value is much greater than the experimental error and, naturally, has to be taken into account if the maximum ω_{LTO} is used as a measure of concentration of isotopes (for more details see Ref. [183]). The measured half-width of the first-order RS line ($\Delta\omega$) is, at middle isotope concentrations, greater in comparison with the endpoints. A complete analogy with what has just been said is observed in the case of the half-width of a 2LO-phonon scattering line in isotopically mixed crystals of $\mathrm{LiH}_x\mathrm{D}_{1-x}$ (Fig. 18a). The maximum value of the half-width of the scattering line is, in both cases, observed in the vicinity of $x = 70\%$. The calculated $\Delta\omega$ in the CPA model is a contribution to the half-width of the RS line in diamond due to the isotopically disordered crystal lattice. According to Hass et al. [183], the observed half-width includes, in addition to the contribution due to the instrumental resolution ($\sim 1.8\ \mathrm{cm}^{-1}$), the anharmonic one. The anharmonicity-related line broadening constitutes, according to Wang et al., $\sim 1\ \mathrm{cm}^{-1}$ at 300 K. Assuming that the anharmonic contribution is independent of the concentration of isotopes, we conclude that the CPA model reproduces the experimental results obtained on diamond quite well (see Fig. 19).

Detailed calculation of the shape of the lines in RS spectra of semiconductors has been performed by Spitzer et al. [198]. In their paper, a quantitative agreement with the experimental data on diamond and germanium has been obtained. Comparing the half-widths of the scattering lines in first-order RS spectra in diamond and germanium (see Fig. 13), it is easy to see that the observed line broadening due to isotopic disorder in diamond is much greater than that in germanium. As is known [141], the reason for this is that the $\mathbf{k} = 0$ point is not the highest point in the diamond dispersion curve (Fig. 10b), whereas in the case of germanium it is the highest point [202]. The shift of the maximum from the Γ point ($\mathbf{k} = 0$) leads to a much larger density of states in the vicinity of ω_{LTO} in comparison with the normal one calculated by the formula

$$N_{\mathrm{d}} \propto \mathrm{Re}\left(\omega_{\mathrm{LTO}} - \omega + \mathrm{i}\left[\frac{\Delta\omega_{\mathrm{LTO}}}{2}\right]\right)^{1/2}$$

(for more details see Ref. [202]). The density of states in diamond is asymmetric with respect to ω_{LTO}, causing asymmetry in the shape of the scattering line [198]. This asymmetry also leads to the asymmetric concentration dependence of the half-width of the scattering line.

As has been mentioned many times, the isotopic disorder in the crystal lattice lifts the forbiddenness imposed by the quasi-momentum conservation law, thus allowing a contribution to the half-width of the scattering line from other phonons from the domain with the maximum density of states, especially from the TO branches. The two structures observed in the spectrum of first-order RS near 275 and 290 cm^{-1} correspond to the maximum of the density of states of TO phonons, which become active because of the violation of the quasi-momentum conservation law by the isotopic disorder in the crystal lattice (Fig. 20). Theoretical calculations of the observed features are, on the whole, in agreement with experimental data (see, however, Ref. [203]). The effect of the development of an additional structure in RS spectra was observed relatively long ago [204] in isotopically mixed $\mathrm{LiH}_x\mathrm{D}_{1-x}$ crystals (Fig. 21) and, very recently, in isotopically mixed crystals of diamond [198] and α-Sn [177]. The effects caused by isotopic disorder in the crystal lattice in isotopically

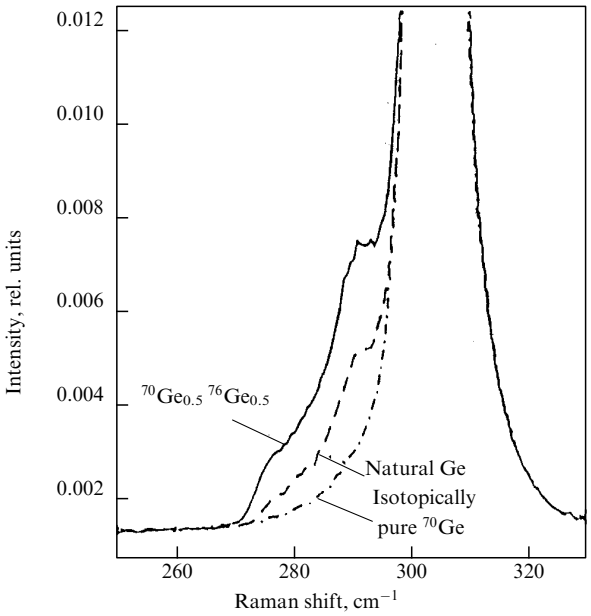

Figure 20. First-order scattering line in Ge, enlarged scale. A contribution of other isotopes is clearly seen [175].

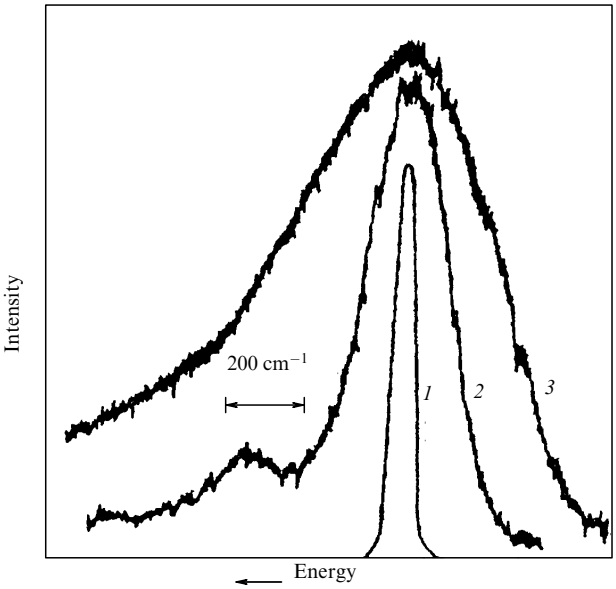

Figure 21. Dependence of the half-width of the line of 2LO(Γ) phonons in RS spectra of (*2*) the pure crystal LiH and (*3*) $\mathrm{LiH}_x\mathrm{D}_{1-x}$. Curve (*1*) shows the profile of the line of exciting light [141].

mixed crystals are analogous to those described above. There exist, however, principal differences (see also Ref. [55]). In contrast to Ge and C, in which the first-order spectra exhibit a one-mode character, the second-order spectra of $\mathrm{LiH}_x\mathrm{D}_{1-x}$ crystals have one- and two-mode characters for LO(Γ) phonons, and also contain a contribution from the local excitation at small values of x. Figure 21 demonstrates the dependence of the half-width of the line of LO(Γ) phonons in light-scattering spectra on the concentration of isotopes. One clearly sees a substantial growth (by a factor of 2–4) of the half-width of the line with increasing concentration of isotopes, as well as the existence of a short-wavelength

structure that has already been related in Ref. [204] to the excitation of TO phonons in isotopically disordered crystal lattice (for more details see Ref. [200]).

5. Conclusions

In this review, we have presented the results of experimental and theoretical studies of the influence of isotope substitution effects and crystal lattice disorder on the elastic, thermal, and vibrational properties of semiconducting and dielectric crystals. The limited applicability of the traditional approach in finding the energy spectrum of disordered systems, when it is possible to separate the potential into ordered and mildly disordered parts, becomes evident. This approach, which works very well for weak phonon scattering in isotopically mixed crystals of diamond and germanium, is not capable of describing media with strong scattering potential (as, for example, in LiH_xD_{1-x} crystals), which induces LO(Γ) phonon localization in such systems. From this, there follows a necessity of developing such an approach that would lead to a self-consistent model of lattice dynamics, within which a unified description of not only local (small concentration range), but also crystal vibrations of mixed crystals in the whole range of the component's concentrations will be possible. A more consistent way of accounting for anharmonicity, beginning, probably, already from the isotope-defect model, is also required. Without such an approach it is impossible to describe neither elastic nor vibrational properties of isotopically mixed crystals. Our view is that it is precisely the consistent way of treating anharmonicity that will allow us to develop such a model of lattice dynamics and will make it possible to describe not only weak, but also strong scattering of phonons due to isotopic disorder. Concluding this short section, it is impossible to refrain from mentioning the applied aspect of the problem considered in this review. As mentioned in the short review [32], wide possibilities of isotope engineering open broad perspectives for its application in solid-state and quantum electronics, materials science, the production of memory elements for modern personal computers, and the development of quantum computers [205].

References

1. Soddy F *Nature* **91** 57 (1913)
2. Holleman A F, Wiberg E *Lehrbuch der anorganischen Chemie* 8th ed. (Berlin: Walter de Gruyter Verlag, 1976); Firestone R B et al. (Eds) *Table of Isotopes* Vol. I, II (New York: Wiley, 1996)
3. Bauche J, Champean R-J *Adv. Atom. Mol. Phys.* **12** 38 (1976)
4. Muller A, in *Advances in Infrared and Raman Spectroscopy* (Eds R J H Clark, R E Hester) Vol. 2 (London: Heyden, 1977) p. 161
5. Herzberg G *Molekulspektren und Molekulstruktur* (Dresden: T. Steinkopff, 1939) [Translated into English: *Molecular Spectra and Molecular Structure* Vol. 1 *Diatomic Molecules* (New York: Prentice-Hall, 1939); translated into Russian (Moscow: IL, 1949)]
6. Bethe H A, Bacher R F *Rev. Mod. Phys.* **8** 82 (1936)
7. Plekhanov V G *Fiz. Tverd. Tela* **37** 1380 (1995) [*Phys. Solid State* **37** 749 (1995)]
8. Ubbelohde A R *Trans. Faraday Soc.* **32** 525 (1936); Robertson J M, Ubbelohde A R *Proc. R. Soc. London Ser. A* **170** 222 (1939)
9. Kogan V S *Usp. Fiz. Nauk* **78** 579 (1962) [*Sov. Phys. Usp.* **5** 260 (1962)]
10. *Laser Applications in Chemistry* (Proc. SPIE, Vol. 669, Ed. D K Evans) (Bellingham, Wash.: The Society, 1986)
11. Pretzel F E et al. *J. Phys. Chem. Solids* **16** 10 (1960)
12. Tyutyunnik O I et al. *J. Cryst. Growth* **68** 741 (1984)
13. Kreĭngol'd F I, Lider K F, Solov'ev L E P*is'ma Zh. Eksp. Teor. Fiz.* **23** 679 (1976) [*JETP Lett.* **23** 624 (1976)]
14. Kreĭngol'd F I, Lider K F, Sapega V F *Fiz. Tverd. Tela* **19** 3158 (1977)
15. Kreĭngol'd F I *Fiz. Tverd. Tela* **27** 2839 (1985) [*Sov. Phys. Solid State* **27** 1712 (1985)]
16. Kreĭngol'd F I *Fiz. Tverd. Tela* **20** 3138 (1978) [*Sov. Phys. Solid State* **20** 1810 (1978)]
17. Kreĭngol'd F I, Kulinkin B S *Fiz. Tverd. Tela* **28** 3164 (1986)
18. Kreĭngol'd F I, Lider K F, Shabaeva M B *Fiz. Tverd. Tela* **26** 3490 (1984)
19. Chrenko R M *J. Appl. Phys.* **63** 5873 (1988)
20. Collins A T et al. *Phys. Rev. Lett.* **65** 891 (1990)
21. Agekyan V F et al. *Fiz. Tverd. Tela* **31** (12) 101 (1989) [*Sov. Phys. Solid State* **31** 2088 (1989)]
22. Itoh K et al. *J. Mater. Res.* **8** 1341 (1993)
23. Pavone P, Baroni S *Solid State Commun.* **90** 295 (1994)
24. Göbel A et al. *Phys. Rev. B* **56** 210 (1997)
25. Serrano J et al. *Phys. Rev. B* **64** 045201 (2001)
26. Takyu K et al. *Jpn. J. Appl. Phys. Pt. 2* **38** L1493 (1999)
27. Garro N et al. *Phys. Rev. B* **54** 4732 (1996)
28. Plekhanov V G, Altukhov V I, in *Proc of the. Intern. Conf. LASERS'82* (McLean, VA: STS Press, 1983) p. 292; Plekhanov G V, in *Proc. of the Intern. Conf. on Advanced Solid-State Lasers, Salt Lake City, UT, USA, March 5–7, 1990* (Washington, DC: Optical Society of America, 1990) p. 132
29. Ginzburg V L *Usp. Fiz. Nauk* **118** 315 (1976) [*Sov. Phys. Usp.* **19** 174 (1976)]; Plekhanov V G *Opt. Spektrosk.* **69** 822 (1990) [*Opt. Spectrosc.* **69** 489 (1990)]
30. Berezin A A *J. Phys. Chem. Solids* **50** 5 (1989)
31. Haller E E *J. Appl. Phys.* **77** 2857 (1995); Magerle R et al. *Phys. Rev. Lett.* **75** 1594 (1995); Kuriyama K, Sakai K, Okada M *Phys. Rev. B* **53** 987 (1996)
32. Plekhanov V G *Usp. Fiz. Nauk* **170** 1245 (2000) [*Phys. Usp.* **43** 1147 (2000)]
33. Lifshitz I M *Fizika Real'nykh Kristallov i Neuporyadochennykh Sistem. Izbrannye Trudy* (Physics of Real Crystals and Disordered Systems. Selected Works (Eds M I Kaganov, A M Kosevich) (Moscow: Nauka, 1987)
34. Maradudin, A A, Montroll E W, Weiss G H *Theory of Lattice Dynamics in the Harmonic Approximation* (Solid State Physics, Suppl. 3) (New York: Academic Press, 1963) [Translated into Russian (Moscow: Mir, 1965)]
35. Dean P *Rev. Mod. Phys.* **44** 127 (1972)
36. Bell R J *Rep. Prog. Phys.* **35** 1315 (1972)
37. Taylor D W, in *Dynamical Properties of Solids* Vol. 2 *Crystalline Solids, Applications* (Eds G K Horton, A A Maradudin) (Amsterdam: North-Holland Publ. Co., 1975) Ch. 5
38. Barker A S (Jr.), Sievers A J *Rev. Mod. Phys.* **47** (Suppl. 2) S1 (1975)
39. Thorpe M F (Ed.) *Excitations in Disordered Systems* (NATO Adv. Study Institutes Series, Ser. B, Vol. 78) (New York: Plenum Press, 1982)
40. Klein M V, in *Dynamical Properties of Solids* Vol. 6 *The Modern Physics of Phonons* (Eds G K Horton, A A Maradudin) (Amsterdam: North-Holland, 1990) Ch. 2
41. Chang I F, Mitra S S *Adv. Phys.* **20** 360 (1971)
42. Elliott R J, Krumhansl J A, Leath P L *Rev. Mod. Phys.* **46** 465 (1974)
43. Taylor D W, in *Excitations in Disordered Systems* (NATO Adv. Study Institutes Series, Ser. B, Vol. 78, Ed. M F Thorpe) (New York: Plenum Press, 1982) p. 182
44. Zimmerman W B *Phys. Rev. B* **5** 4704 (1972)
45. Holloway H et al. *Phys. Rev. B* **44** 7123 (1991)
46. Yamanaka T, Morimoto S, Kanda H *Phys. Rev. B* **49** 9341 (1994)
47. Brodsky M H (Ed.) *Amorphous Semiconductors* (Topics in Applied Physics, Vol. 36) (Berlin: Springer-Verlag, 1979) [Translated into Russian (Moscow: Mir, 1982)]
48. Kirkpatrick S *Rev. Mod. Phys.* **45** 574 (1973)
49. Plekhanov V G *Phys. Rev. B* **51** 8874 (1995)
50. Cowley R A *Adv. Phys.* **12** 421 (1963); Cochran W, Cowley R A, in *Encyclopedia of Physics* (Ed. L Genzel) (Berlin: Springer-Verlag, 1967) p. 59
51. Cochran W *The Dynamics of Atoms in Crystals* (The Structures and Properties of Solids, Vol. 3) (London: Edward Arnold, 1973)

52. Leibfried G, Ludwig W *Theory of Anharmonic Effects in Crystals* (New York: Academic Press, 1961) [Translated into Russian (Moscow: IL, 1963)]
53. Reissland J A *The Physics of Phonons* (London: John Wiley and Sons, 1973) [Translated into Russian (Moscow: Mir, 1975)]
54. Calder R S et al. *J. Phys. Chem. Solids* **23** 621 (1962)
55. Plekhanov V G *Opt. Spektrosk.* **82** 105 (1997) [*Opt. Spectrosc.* **82** 95 (1997)]
doi 56. Plekhanov V G *Usp. Fiz. Nauk* **167** 577 (1997) [*Phys. Usp.* **40** 553 (1997)]
57. Vavilov V S, Gippius A A, Konorova E A *Elektronnye i Opticheskie Protsessy v Almaze* (Electron and Optical Processes in Diamond) (Moscow: Nauka, 1985)
doi 58. Baroni S et al. *Rev. Mod. Phys.* **73** 515 (2001)
doi 59. Zhernov A P, Inyushkin A V *Usp. Fiz. Nauk* **171** 827 (2001); **172** 573 (2002) [*Phys. Usp.* **44** 785 (2001); **45** 527 (2002)]
60. Musgrave M J P *Crystal Acoustics*; *Introduction to the Study of Elastic Waves and Vibrations in Crystals* (San Francisco: Holden-Day, 1970)
61. Nye J F *Physical Properties of Crystals, Their Representation by Tensors and Matrices* (Oxford: Clarendon Press, 1957)
62. Neighbours J R, Schacher G E *J. Appl. Phys.* **38** 5366 (1967)
63. Gluyas M, Hunter R, James B W *J. Phys. C: Solid State Phys.* **8** 271 (1975)
64. James B W, Kheyrandish H *J. Phys. C: Solid State Phys.* **15** 6321 (1982)
65. Born M, Kun H *Dynamical Theory of Crystal Lattices* (Oxford: Clarendon Press, 1954) [Translated into Russian (Moscow: IL, 1958)]
66. Hayes W, Loudon R *Scattering of Light by Crystals* (New York: Wiley, 1978)
67. Sandercock J, in *Festkörperprobleme* (Advances in Solid State Physics) (Braunschweig: Vieweg, 1975) p. 183
68. Guinan M W, Cline C F *J. Nonmetals* **1** 11 (1972)
69. Gerlich D, Smith C S *J. Phys. Chem. Solids* **35** 1587 (1974)
70. Plekhanov V "Isotope Effects in Solid State Physics", in *Semiconductors and Semimetals* Vol. 68 (Eds R K Willardson, E Weber) (New York: Academic Press, 2001)
71. Haussuhl S, Skorzyk W *Z. Kristallogr.* **130** 340 (1969)
72. Leibfried G *Gittertheorie der mechanischen und thermischen Eigenschaften der Kristalle* (Berlin: Springer, 1955) [Translated into Russian: *Mikroskopicheskaya Teoriya Mekhanicheskikh i Teplovykh Svoĭstv Kristallov* (Microscopic Theory of Mechanical and Thermal Properties of Crystals) (Moscow: Fizmatgiz, 1963)]
doi 73. Wilson W D, Johnson R A *Phys. Rev. B* **1** 3510 (1970)
doi 74. Vacher R, Boissier M, Laplaze D *Solid State Commun.* **37** 533 (1981)
doi 75. Herchen H, Cappelli M A *Phys. Rev. B* **43** 11740 (1991)
76. Dyck W *J. Phys. C: Solid State Phys.* **14** 4193 (1981)
doi 77. Debernardi A, Cardona M *Phys. Rev. B* **54** 11305 (1996)
doi 78. Hass K C et al. *Phys. Rev. B* **45** 7171 (1992)
doi 79. Ramdas A K et al. *Phys. Rev. Lett.* **71** 189 (1993)
doi 80. Hurley D C, Gilmore R S, Banholzer W F *J. Appl. Phys.* **76** 7726 (1994)
doi 81. Vogelgesang R et al. *Phys. Rev. B* **54** 3989 (1996)
doi 82. Zouboulis E S et al. *Phys. Rev. B* **57** 2889 (1998)
83. Musgrave M J P, Pople J A *Proc. R. Soc. London Ser. A* **268** 474 (1962)
doi 84. Keating P N *Phys. Rev.* **145** 637 (1966)
doi 85. Martin R M *Phys. Rev. B* **1** 4005 (1970)
doi 86. Holloway H et al. *Phys. Rev. B* **45** 6353 (1992)
87. Mykolajewycz R, Kalnajs J, Smakula A *J. Appl. Phys.* **35** 1773 (1964)
88. Plekhanov V G *Fiz. Tverd. Tela* **37** 289 (1995) [*Phys. Solid State* **37** 157 (1995)]
doi 89. Plekhanov V G *J. Raman Spectrosc.* **32** 631 (2001)
90. Laplaze D, Boisser M, Vacher R *Solid State Commun.* **19** 445 (1976)
91. Laplaze D *J. Phys. C: Solid State Phys.* **10** 3499 (1977)
92. Terras C, Moussin C *CR Acad. Sci. A* **272** 815 (1971)
93. Stephens D R, Lilley E M *J. Appl. Phys.* **39** 177 (1968)
94. Johnston Q, Mitchell A C, Evans L *Acta Crystallogr. A* **31** S241 (1975)
95. Jex H *J. Phys. Chem. Solids* **35** 1221 (1974)
96. Ghosh S, Basu A N, Sengupta S *Phys. Status Solidi B* **103** 595 (1981)
97. Kostryukov V N *Zh. Fiz. Khim.* **35** 1759 (1961)
98. Yates B, Wostenholm G H, Bingham J L *J. Phys. C: Solid State Phys.* **7** 1769 (1974)
99. Catalana E, Leider H R *J. Phys. Chem. Solids* **32** 1297 (1971)
100. Laplaze D *Phys. Status Solidi B* **91** 59 (1979)
101. Laplaze D *J. Phys.* (Paris) **3** 105 (1976)
102. Klemens P G, in *Solid State Physics: Advances in Research and Applications* Vol. 7 (Eds F Seits, D Turnbull) (New York: Academic Press, 1958) p. 1
doi 103. Holland M G *Phys. Rev.* **132** 2461 (1963); in *Physics of III–V Compounds* (Semiconductors and Semimetals, Vol. 2, Eds R K Willardson, A C Beer) (New York: Academic Press, 1966) p. 3
104. Touloukian Y S et al. *Thermal Conductivity: Metallic Elements and Alloys* (Thermophysical Properties of Matter, Vol. 1, Ed. Y S Touloukian) (New York: IFI/Plenum, 1970) p. 108
105. Hellwege K-H, Madelung O (Eds) *Landolt-Börnstein, New Series. Semiconductors, Intrinsic Properties of Group IV Elements, and III–V–VI and I–VII Compounds* Vol. 22, Pt. A (Berlin: Springer, 1987) p. 281
106. Berman R *Z. Phys. Chemie. Neue Fol.* **16** 10 (1958)
107. Peierls R E *Quantum Theory of Solids* (Oxford: Clarendon Press, 1955)
108. Ziman J M *Models of Disorder* (Cambridge: Cambridge Univ. Press, 1979)
doi 109. Callaway J *Phys. Rev.* **113** 1046 (1959)
110. Berman R *Thermal Conduction in Solids* (Oxford: Clarendon Press, 1976) [Translated into Russian (Moscow: Mir, 1979)]
doi 111. Herring C *Phys. Rev.* **95** 954 (1954)
doi 112. Nelin G, Nilsson G *Phys. Rev. B* **5** 3151 (1972)
doi 113. Olson J R et al. *Phys Rev. B* **47** 14850 (1993)
114. Pomeranchuk I Ya *J. Phys. USSR* **6** 237 (1942); *Zh. Eksp. Teor. Fiz.* **12** 245 (1942)
doi 115. Geballe T H, Hull G W *Phys. Rev.* **110** 773 (1958)
doi 116. Anthony T R et al. *Phys. Rev. B* **42** 1104 (1990)
doi 117. Banholzer W F, Anthony T R *Thin Solid Films* **212** 1 (1992)
doi 118. Onn D G et al. *Phys. Rev. Lett.* **68** 2806 (1992)
doi 119. Belay K et al. *J. Appl. Phys.* **79** 8336 (1996)
doi 120. Graebner J E et al. *Phys. Rev. B* **50** 3702 (1994)
doi 121. Asen-Palmer M et al. *Phys. Rev. B* **56** 9431 (1997)
doi 122. Zhernov A P *Fiz. Tverd. Tela* **44** 992 (2002) [*Phys. Solid State* **44** 1035 (2002)]
doi 123. Capinski W S et al. *Appl. Phys. Lett.* **71** 2109 (1997)
doi 124. Capinski W S, Maris H J, Tamura S *Phys. Rev. B* **59** 10105 (1999)
doi 125. Ruf T et al. *Solid State Commun.* **115** 243 (2000)
126. Novikov N V (Ed.) *Fizicheskie Svoĭstva Almaza*. Spravochnik (Physical Properties of Diamond. Handbook) (Kiev: Naukova Dumka, 1987)
127. Omini M, Sparavigna A *Nuovo Cimento D* **19** 1537 (1997)
doi 128. Zhernov A P *Zh. Eksp. Teor. Fiz.* **120** 1237 (2001) [*JETP* **93** 1074 (2001)]
doi 129. Muinov M, Kanda H, Stishov S M *Phys. Rev. B* **50** 13860 (1994)
130. Kogan V S, Omarov G G *Fiz. Tverd. Tela* **7** 3 (1965)
131. Baĭkov Yu M et al. *Fiz. Tverd. Tela* **11** 3050 (1969) 1
doi 132. Smith D K, Leider H R *J. Appl. Crystallogr.* **1** 246 (1968)
133. London G *Z. Phys. Chemie. Neue Fol.* **16** 302 (1958)
doi 134. Anderson J L et al. *J. Phys. Chem. Solids* **31** 613 (1970)
doi 135. Ruffa A R *Phys. Rev. B* **27** 1321 (1983)
136. Tyutyunnik V I *Phys. Status Solidi B* **172** 539 (1992)
137. Tyutyunnik V I *Phys. Status Solidi B* **181** 373 (1994)
138. Mel'nikova T I *Fiz. Tverd. Tela* **22** 588 (1980)
139. Shpil'raĭn E E, Yakimovich K A, Mel'nikova T I *Teplofizicheskie Svoĭstva Gidrida, Deĭterida i Tritida Litiya i Ikh Rastvorov s Litiem* (Thermophysical Properties of Lithium Hydride, Deuteride, and Tritide and of Their Solutions with Lithium) (Moscow: Energoatomizdat, 1983) [Translated into English (New York: American Institute of Physics, 1987)]
doi 140. Berezin A A, Ibrahim A M *Mater. Chem. Phys.* **19** 407 (1988)
doi 141. Plekhanov V G *Mater. Sci. Eng. R.* **35** 139 (2001)
doi 142. Plekhanov V G, Plekhanov N V *Phys. Lett. A* **313** 231 (2003)
doi 143. Buschert R C et al. *Phys. Rev. B* **38** 5219 (1988)
doi 144. Noya J C, Herrero C P, Ramírez R *Phys. Rev. B* **56** 237 (1997)
doi 145. Kazimirov A, Zegenhagen J, Cardona M *Science* **282** 930 (1998)
doi 146. Herrero C P *Solid State Commun.* **110** 243 (1999)

147. Banholzer W, Anthony T R, Gilmore R, in *New Diamond Science and Technology*: *Proc. of the 2nd Intern. Conf., Washington, DC, USA, Sept. 23–27, 1990* (MRS Conf. Proc., Eds R Messier et al.) (Pittsburgh, Pa.: Materials Research Society, 1991) p. 857
148. Von Dreele R B, Morgan J G, Stishov S M *Zh. Eksp. Teor. Fiz.* **114** 2182 (1998) [*JETP* **87** 1188 (1998)]; Stishov S M *Usp. Fiz. Nauk* **171** 299 (2001) [*Phys. Usp.* **44** 285 (2001)]
149. Krivoglaz M A *Teoriya Rasseyaniya Rentgenovskikh Lucheĭ i Teplovykh Neĭtronov Real'nymi Kristallami* (Theory of X-Ray and Thermal-Neutron Scattering by Real Crystals) (Moscow: Nauka, 1967) [Translated into English (New York: Plenum Press, 1969)]
150. Dolling G, in *Dynamical Properties of Solids* Vol. 1 *Crystalline Solids, Fundamentals* (Eds G K Horton, A A Maradudin) (Amsterdam: North-Holland, 1974) p. 541
151. Zemlianov M G et al., in *Inelastic Scattering in Neutrons*: *Proc. Symp., Bombay, India, 1964* Vol. 2 (Vienna: IAEA, 1965) p. 431
152. Verble J L, Warren J L, Yarnell J L *Phys. Rev.* **168** 980 (1968)
153. Pilipenko G I, Tyutyunnik O I, Gavrilov F F *Zh. Prikl. Spektrosk.* **42** 657 (1985)
154. Warren J L et al. *Phys. Rev.* **158** 805 (1967)
155. Dolling G, Woods A D B, in *Thermal Neutron Scattering* (Ed. P A Egelstaff) (London: Academic Press, 1965) p. 193
156. Nilsson G, Nelin G *Phys. Rev. B* **3** 364 (1971)
157. Tubino R, Piseri L, Zerbi G *J. Chem. Phys.* **56** 1022 (1972)
158. Bilz H, Kress W *Phonon Dispersion Relations in Insulators* (Springer Ser. in Solid-State Sci., Vol. 10) (Berlin: Springer-Verlag, 1979)
159. Schwoerer-Böhning M, Macrander A T, Arms D A *Phys. Rev. Lett.* **80** 5572 (1998)
160. Windl W et al. *Phys. Rev. B* **48** 3164 (1993)
161. Kulda J et al. *Solid State Commun.* **99** 799 (1996)
162. Pavone P et al. *Phys. Rev. B* **48** 3156 (1993)
163. Andreev A F *Usp. Fiz. Nauk* **118** 251 (1976) [*Sov. Phys. Usp.* **19** 137 (1976)]
164. Lifshitz I M *Nuovo Cimento Suppl.* **3** 716 (1956)
165. Lifshitz I M, Kosevich A M *Rep. Prog. Phys.* **29** 217 (1966)
166. Jaswal S S, Wolfram G, Sharma T P *J. Phys. Chem. Solids* **35** 571 (1974)
167. Anderson A, Lüty F *Phys. Rev. B* **28** 3415 (1983)
168. Plekhanov V G *Solid State Commun.* **76** 51 (1990)
169. Jaswal S S, Sharma T P, Wolfram G *Solid State Commun.* **11** 1151 (1972)
170. Elliott R J, Taylor D W *Proc. R. Soc. London Ser. A* **296** 161 (1967)
171. Jaswal S S, Hardy J R *Phys. Rev.* **171** 1090 (1968)
172. Ho A C, Ph.D. Thesis (Tempe, AZ: Arizona State Univ., 1996)
173. Nordheim L *Ann. Phys.* (Leipzig) **9** 641 (1931)
174. Pant M M, Joshi S K *Phys. Rev.* **184** 635 (1969)
175. Cardona M et al. *J. Phys.*: *Condens. Matter* **5** A61 (1993); Fuchs H D et al. *Phys. Rev. Lett.* **70** 1715 (1993)
176. Zhang J M et al. *Phys. Rev. B* **57** 1348 (1998)
177. Wang D T et al. *Phys. Rev. B* **56** 13167 (1997)
178. Lax M, Burstein E *Phys. Rev.* **97** 39 (1955)
179. Zhang J M et al. *Phys. Rev. B* **57** 9716 (1998)
180. Hanzawa H et al. *Phys. Rev. B* **54** 3793 (1996)
181. Cardona M, in *Festkörperprobleme* (Advances in Solid State Physics, Vol. 34, Ed. R Helbig) (Braunschweig: Vieweg, 1994) p. 34; Widulle F et al. *Physica B* **263** 381 (1999)
182. Göbel A et al. *Phys. Rev. Lett.* **77** 2591 (1996)
183. Hass K C et al. *Phys. Rev. B* **44** 12046 (1991)
184. Solin S A, Ramdas A K *Phys. Rev. B* **1** 1687 (1970)
185. Fuchs H D et al. *Phys. Rev. B* **43** 4835 (1991)
186. Fuchs H D et al. *Solid State Commun.* **82** 225 (1992)
187. Tyutyunnik V I, Tyutyunnik O I *Phys. Status Solidi B* **162** 597 (1990)
188. Plekhanov V G *Opt. Spektrosk.* **76** 65 (1994) [*Opt. Spectrosc.* **76** 59 (1994)]
189. Ipatova I P, in *Optical Properties of Mixed Crystals* (Modern Problems in Condensed Matter Sciences, Vol. 23, Eds R J Elliott, I P Ipatova) Ch. 1 (Amsterdam: North-Holland, 1988) p. 1
190. Plekhanov V G *Opt. Spektrosk.* **75** 51 (1993) [*Opt. Spectrosc.* **75** 31 (1993)]
191. Plekhanov V G *Pis'ma Zh. Tekh. Fiz.* **14** 303 (1988) [*Sov. Tech. Phys. Lett.* **14** 134 (1988)]
192. Montgomery D J, Hardy J R, in *Lattice Dynamics*: *Proc. of the Intern. Conf., Copenhagen, Denmark, Aug. 5–9, 1963* (Suppl. to the J. Phys. Chem. Solids, Suppl. 1, Ed. R F Wallis) (Oxford: Pergamon Press, 1965) p. 491
193. Behera S N, Tripathi R S *J. Phys. C*: *Solid State Phys.* **7** 4452 (1974)
194. Elliott R J, Leath P L, in *Dynamical Properties of Solids* Vol. 2 *Crystalline Solids, Applications* (Eds G K Horton, A A Maradudin) (Amsterdam: North-Holland Publ. Co., 1975) p. 385
195. Taylor D W *Phys. Rev.* **156** 1017 (1967)
196. Ehrenreich H, Schwartz L M "The Electronic Structure of Alloys", in *Solid State Physics* Vol. 31 (Eds H Ehrenreich, F Seitz, D Turnbull) (New York: Academic Press, 1976) p. 149
197. Taylor D W, in *Optical Properties of Mixed Crystals* (Modern Problems in Condensed Matter Sciences, Vol. 23, Eds R J Elliott, I P Ipatova) Ch. 2 (Amsterdam: North-Holland, 1988) p. 35
198. Spitzer J et al. *Solid State Commun.* **88** 509 (1993)
199. Efros A L, Raikh M E, in *Optical Properties of Mixed Crystals* (Modern Problems in Condensed Matter Sciences, Vol. 23, Eds R J Elliott, I P Ipatova) Ch. 5 (Amsterdam: North-Holland, 1988) p. 135
200. Plekhanov V G *Prog. Solid State Chem.* **29** 71 (2001)
201. Wang C Z, Chang C T, Ho K M *Solid State Commun.* **76** 483 (1990)
202. Cardona M *Phys. Status Solidi B* **220** 5 (2000)
203. Göbel A et al. *Phys. Rev. B* **58** 10510 (1998)
204. Plekhanov V G, Altukhov V I *J. Raman Spectrosc.* **16** 358 (1985)
205. Nielsen M A, Chuang I L *Quantum Computation and Quantum Information* (Cambridge: Cambridge Univ. Press, 2000)